Title

Regulatory T cells in skin mediate immune privilege of the hair follicle stem cell niche

Journal

Science Immunology, 9(91)

ISSN

2470-9468

Authors

Cohen, Jarish N
Gouirand, Victoire
Macon, Courtney E
et al.

Publication Date

2024-01-12

DOI

10.1126/sciimmunol.adh0152

Peer reviewed

HHS Public Access

Author manuscript

Sci Immunol. Author manuscript; available in PMC 2024 April 10.

Published in final edited form as:

Sci Immunol. 2024 January 05; 9(91): eadh0152. doi:10.1126/sciimmunol.adh0152.

Regulatory T cells in skin mediate immune privilege of the hair follicle stem cell niche

Jarish N. Cohen[1,2], **Victoire Gouirand**[1], **Courtney E. Macon**[1], **Margaret M. Lowe**[1], **Ian C. Boothby**[1,3], **Joshua M. Moreau**[1], **Iris K. Gratz**[4], **Angelika Stoecklinger**[4,5], **Casey T. Weaver**[6], **Arlene H. Sharpe**[7,8,9], **Roberto R. Ricardo-Gonzalez**[1], **Michael D. Rosenblum**[1,*]

[1]Department of Dermatology, University of California, San Francisco, San Francisco, CA, USA

[2]Department of Pathology, University of California, San Francisco, San Francisco, CA, USA

[3]Medical Scientist Training Program, University of California, San Francisco, CA, USA

[4]Department of Molecular Biology, University of Salzburg, Salzburg, Austria

[5]EB House Austria, Research Program for Molecular Therapy of Genodermatoses, Department of Dermatology, University Hospital of the Paracelsus Medical, University of Salzburg, Salzburg, Austria

[6]Department of Pathology, University of Alabama at Birmingham, Birmingham, AL, USA

[7]Department of Immunology, Blavatnik Institute, Harvard Medical School, Boston, MA, USA

[8]Evergrande Center for Immunological Diseases, Harvard Medical School and Brigham and Women's Hospital, Boston, MA, USA

[9]Department of Pathology, Brigham and Women's Hospital, Boston, MA, USA

Abstract

Immune tolerance is maintained in lymphoid organs (LOs). Despite the presence of complex immune cell networks in non-LOs, it is unknown if self-tolerance is maintained in these tissues. We developed a technique to restrict genetic recombination to regulatory T cells (Tregs) only in skin. Selective depletion of skin Tregs resulted in T cell-mediated inflammation of hair follicles (HF). Suppression did not rely on CTLA-4, but instead on high affinity interleukin-2 (IL-2) receptor expression by skin Tregs, functioning exclusively in a cell-extrinsic manner. In a novel model of HF stem cell (HFSC) driven autoimmunity, we reveal that skin Tregs immunologically protect the HFSC niche. Finally, we utilized spatial transcriptomics to identify aberrant IL-2 signaling at stromal-HF interfaces in a rare form of human alopecia characterized by HFSC

[*]**Address of Correspondence:** Michael D. Rosenblum M.D., Ph.D., Medical Sciences Building, Health Sciences West - 1201B, 513 Parnassus Avenue, San Francisco, CA 94132, Michael.Rosenblum@ucsf.edu.

Author contributions: Conceptualization: J.N.C. and M.D.R. Methodology: J.N.C., R.R.R-G., M.D.R. Investigation: J.N.C., I.C.B., J.M.M., V.G., C.E.M Resources: M.D.R., I.K.G., A.S., C.T.W., A.H.S. Data Curation: J.N.C. Writing- Original Draft: J.N.C. Writing-Editing and Revision: J.N.C. and M.D.R. Supervision: M.D.R.

Competing interests: M.D.R. is a consultant and co-founder of TRex Bio Inc., Sitryx Bio Inc., and Radera Bio Inc. He is also a consultant for Mozart Bio Inc. J.N.C. is a consultant for TRex Bio Inc and Radera Bio Inc. All other authors declare no competing interests.

destruction and Alopecia Areata. Collectively, these results reveal the fundamental biology of Tregs in skin uncoupled from the systemic pool and elucidate a mechanism of self-tolerance.

One-sentence summary:

Skin-specific manipulation of regulatory T cells uncovers a role in protecting hair follicle stem cells from autoimmune attack.

Introduction

Tolerance mechanisms prevent self-reactive lymphocytes from inciting autoimmunity. In the thymus, developing T cells with potential autoreactivity are largely purged from the nascent repertoire(1). This process, known as ‘central’ tolerance, is partially reliant on display of peripheral tissue antigens by specialized epithelial cells in the thymic medulla *via* expression of the autoimmune regulator (Aire)(2). However, central tolerance is imperfect, as numerous self-reactive T cell clones escape thymic selection(3). The immune system has evolved mechanisms in secondary lymphoid organs (LOs) to control autoreactive T cells that have escaped thymic selection, a process known as ‘peripheral’ tolerance. Presentation of self-antigen in the steady-state by immature dendritic cells or lymph node (LN) stromal cells can lead to deletion or functional non-responsiveness (anergy) of autoreactive T cells(4, 5). Regulatory T cells (Tregs) are specialized CD4+ lymphocytes that enforce tolerance in secondary LOs, where initial antigen encounter and T cell priming occur(6). The role of Tregs as critical mediators of self-tolerance is exemplified by fatal multi-organ autoimmunity in mice following their depletion(7, 8).

Tregs are also present in significant numbers in non-LOs, such as skin and gut(9, 10), suggesting that they may also play an immunoregulatory role in these tissues. In humans, mutations in *FOXP3* results in a systemic autoimmune syndrome termed Immune Dysregulation, Polyendocrinopathy, Enteropathy, X-linked (IPEX)(11). Resulting from Treg dysfunction, skin manifestations of IPEX include various dermatoses and autoimmune alopecia(12, 13). Interestingly, a subset of skin Tregs localize to hair follicles (HFs) in mice and humans, with some showing a proclivity for the bulge region where HF stem cells (HFSCs) reside(10, 14). However, it is currently unknown how long these cells persist in skin and whether they play an active role in protecting HFSCs from autoimmune attack. Understanding how tissue resident Tregs function is needed to fully uncover the biology of these cells and selectively manipulate them for therapeutic benefit.

A major obstacle in discerning the function of Tregs (and other immune cells) that reside in specific tissues has been the inability to selectively manipulate these cells without perturbing cells of the same lineage that reside elsewhere in the body. Experimental models that investigate Treg biology have traditionally relied on mice expressing the human diphtheria toxin receptor (DTR)(7, 8), a Tamoxifen-inducible Cre recombinase (Cre^{ERT2})(15), or a constitutive Cre recombinase under the control of the Foxp3 promoter(16, 17). In the former two mouse models, systemic administration of DT or Tamoxifen results in total-body reduction of Tregs or deletion of specific genes in Tregs in all tissues, respectively. Other studies have utilized approaches that prevent Tregs from trafficking to specific non-LOs

using deletion of chemokine or integrin pathways(18, 19). Although eloquent in design, these studies are also hampered by manipulation of the systemic Treg pool and/or adoptive cell transfers into immunodeficient hosts. Thus, the function of tissue resident Tregs has yet to be robustly and comprehensively elucidated due to an inability to selectively manipulate these cells in specific organs in otherwise unmanipulated adult animals. Here, we demonstrate a technique to genetically manipulate Tregs that reside in skin with a high level of specificity. With the ability to deplete Tregs only in skin, we find that a major function of these cells is to preferentially protect HFs from autoimmune attack. In doing so, we define a mechanism of immunologic self-tolerance active in a peripheral non-LO.

Results

Skin-specific gene recombination in Tregs

To overcome the limitation of traditional methods of Treg modulation and address whether they are amenable to selective manipulation in skin, we crossed mice expressing a Tamoxifen inducible Cre recombinase under the control of the Foxp3 promoter (Foxp3-Cre$^{ERT2\text{-}GFP}$)(15) to mice carrying a Rosa26-lox-stop-lox (*LSL*)-tdTomato allele (Foxp3^{tdTomato}; Figure S1A). When administered systemically, Tamoxifen is metabolized in the liver to its active form, Z-4-hydroxytamoxifen (4OHT)(20). Flow cytometric quantification showed that intraperitoneal injection of Tamoxifen in Foxp3^{tdTomato} mice resulted in near complete tdTomato expression in Tregs in skin, other non-LO, and LOs (Figure S1B). We rationalized that if an optimal concentration of 4OHT was directly applied to skin, localized, inducible Cre-mediated genetic recombination only in skin Tregs could be achieved. Thus, varying concentrations of 4OHT were topically applied to shaved dorsal back skin of adult Foxp3^{tdTomato} mice for five consecutive days. Skin and skin-draining LN (SDLN) were harvested 2 days thereafter. While all concentrations of topical 4OHT resulted in similar tdTomato-labeling efficiency of skin Tregs (~70–90%), the 20 μg/ml dose demonstrated minimal labeling (~1%) of Tregs in SDLN (Figures S1C and S1D); this concentration was used in subsequent experiments utilizing Foxp3^{tdTomato} mice.

To test the skin specificity of topical 4OHT treatment more broadly, Foxp3^{tdTomato} mice were shaved in a ‘mohawk’ pattern (Figure 1A) and treated with topical 4OHT on one side and vehicle control (acetone) on contralateral skin (Figure 1B). Two days following the last treatment, skin from both treatment conditions and multiple LOs and non-LOs were harvested. Flow cytometry showed the frequency of tdTomato+ Tregs in 4OHT-treated skin to be ~70–80%. In contrast, those in contralateral vehicle-control treated skin, other barrier tissues, and LOs was equal to or less than 2% (Figure 1C). Immunofluorescence microscopy confirmed that tdTomato+ cells were largely restricted to 4OHT-treated skin (Figure 1D). Importantly, tdTomato was not expressed by CD4+ T effector cells (CD4+ Foxp3−; Teffs), CD8+ T cells, and CD45+ CD3− cells in skin (Figure S2). Collectively, these data demonstrate a topical technique to induce localized, efficient genetic recombination that is largely restricted to Tregs in skin.

Skin Tregs undergo attrition during homeostasis but expand after inflammation

The natural life history of immune cells in healthy peripheral tissues has been difficult to discern, as traditional approaches rely on systemic labeling. We hypothesized that topical 4OHT application could be used to track the fate of Tregs in an unbiased manner in skin of adult mice. Thus, we administered 4OHT topically to Foxp3^{tdTomato} mice using the same treatment scheme as above and harvested skin at defined time points (Figure 1E). Flow cytometry showed that the frequency of tdTomato+ skin Tregs diminish as mice age (Figure 1F and 1G). Nonetheless, ~5–10% of tdTomato+ Tregs persisted in skin at least 100 days after initial labeling. Immunofluorescence microscopy confirmed a numerical attrition of tdTomato+ cells in skin over time (Figure 1H). Together, these data suggest that skin Tregs undergo substantial attrition and continuous replacement in the steady-state, but a small fraction are endowed with the ability to persist long-term.

To determine if skin Tregs persist following cutaneous injury, topical 4OHT was applied to both sides of shaved back skin of Foxp3^{tdTomato} mohawk mice, and skin inflammation was induced on one side of back skin by repeatedly tape-stripping to induce superficial injury while the contralateral side was left unperturbed(21, 22) (Figure S3A). 3 weeks thereafter, skin was harvested. By flow cytometry, four distinct subsets of skin CD4+ T cells could be discerned based on Foxp3 and tdTomato expression: non-labeled Tregs (Foxp3+ tdTomato−), labeled Tregs (Foxp3+ tdTomato+), so-called ‘ex-Tregs’ (Foxp3− tdTomato+), and Teffs (Foxp3− tdTomato−) (Figure S3B). While the frequency of tdTomato+ skin Tregs was reduced after superficial cutaneous injury compared to contralateral non-tape-stripped skin, the overall number of tdTomato+ skin Tregs increased, as did non-labeled Tregs and Teffs (Figures S3C–S3E). No significant numbers of CD4+ Foxp3− tdTomato+ T cells were identified pre- or post-injury, indicating that skin Tregs do not become ex-Tregs in this model of cutaneous inflammation. Overall, we demonstrate that pre-existing skin Tregs accumulate and persist in skin following superficial injury.

Skin Tregs restrain hair follicle-associated inflammation

LOs are believed to be the primary anatomic site of Treg-mediated peripheral immune tolerance(6). This paradigm was established from studies of mice engineered to undergo systemic depletion of Tregs, which results in unrestrained effector T cell activation and multi-organ autoimmunity(7, 8). However, a limitation of this technique is its inability to uncouple the tolerogenic function of Tregs in LOs versus those in non-LOs. To resolve this fundamental question, we crossed Foxp3-Cre$^{ERT2\text{-}GFP}$ mice to mice carrying a Rosa26-*LSL*-diphtheria toxin α (DTA) subunit allele whereby DTA is expressed in Tregs under the influence of 4OHT (Foxp3^{iDTA} mice), ultimately resulting in cell death. Foxp3^{iDTA} mohawk mice were treated topically with 4OHT (or vehicle control) or injected intraperitoneally with Tamoxifen at regular intervals over the course of 4 weeks in an effort to maximize Treg depletion and study its long-term effects (Figure 2A). SDLN in Tamoxifen-treated mice were enlarged in a manner similar to other models of systemic Treg depletion(7, 8), whereas those in mice treated topically with 4OHT remained smaller (Figure 2B). Flow cytometry confirmed ablation of Tregs in SDLN of Tamoxifen-treated mice to levels that were ~50% of those that drained control- or 4OHT-treated skin (Figures 2C and 2D). Importantly, the frequency of Tregs in 4OHT-treated skin was reduced by ~50% compared to that of

contralateral control-treated skin, similar to the level observed in skin of Tamoxifen-treated mice (Figures 2C and 2D). These results demonstrate that an approximate 50% reduction is the maximal Treg depletion achievable using this model, which can be attained specifically in skin *via* topical 4OHT treatment.

A major role of Tregs in LOs is to restrain accumulation and effector function of pro-inflammatory cells. Thus, we assessed these parameters in mice where skin Tregs were selectively reduced. An increased frequency and number of CD8+ T cells and Teff cells was observed in 4OHT- versus control-treated skin at levels comparable to that observed in mice that underwent systemic Treg depletion (Figures 2E–2G). Importantly, no significant difference in the number of CD8+ T cell and Teff was observed in SDLNs that drained either control or contralateral 4OHT-treated skin. Increases in dermal γ/δ T cells and inflammatory Ly6C+ monocytes were also observed in skin depleted of Tregs, while dendritic epidermal T cells (DETCs) and other myeloid subsets did not show significant changes (Figures S4A–S4C). Expression of the co-stimulatory molecules CD80 and CD86 were increased on Langerhans cells in Treg-depleted skin (Figure S4D), indicating that skin Tregs may directly or indirectly suppress activation of these cells in the steady-state and is consistent with previously reported cross-talk between these two cell types(23). Pro-inflammatory cytokine production was enhanced in skin CD8+ T cells and Teffs as evidenced by increased interferon-gamma (IFN-γ) and tumor necrosis factor-alpha (TNF-α) production in Treg-depleted skin, but not by those in SDLN (Figure 2H).

We next evaluated skin for histopathologic evidence of immune-mediated pathology. Strikingly, skin that underwent Treg depletion showed prominent inflammation of HFs (Figure 2I). The increased inflammatory parameters were not due to intrinsic effects of 4OHT, as HF-associated inflammation was not observed in skin of genetic controls (Foxp3-Cre^{ERT2}) treated topically with this molecule (Figure S5A–S5E). Additionally, topical 4OHT treatment over the course of 2-weeks resulted in a similar level of skin Treg depletion and folliculitis compared to the 4-week regimen, indicating that subacute loss of skin Tregs is sufficient to disrupt cutaneous immune homeostasis (Figure S5F–S5H). By depleting CD8+ cells during the topical 4OHT treatment regimen (Figure 2J), we found that HF-associated inflammation was partially abrogated (Figure 2K). It is unlikely that CD8-expressing dendritic cells (DC) influenced this phenotype, since this DC subset is not present in skin(24) and the antibody depletion approach implemented does not completely eliminate this cell type compared to CD8+ T cells(25). Collectively, these results demonstrate a methodology to selectively deplete pre-existing Tregs in a non-LO, which revealed that skin-resident Tregs restrain cutaneous autoimmunity in the steady-state, in part by suppressing CD8+ T cell-mediated HF inflammation. Additionally, our results show that skin is exquisitely sensitive to perturbations in resident Tregs, as only partial reduction (~50%) can result in overt HF-associated inflammation.

To determine if pre-existing T cells in skin cause autoinflammatory pathology following skin Treg depletion, mohawk Foxp3^{iDTA} mice were treated with either topical vehicle control or 4OHT. Additionally, one group of mice received intraperitoneal injections of the sphingosine 1-phosphate receptor-1 modulator, FTY720, every 3 days to block egress of lymphocytes out of LOs into circulation, which we confirmed by detection of increased

TCRβ+ T cells in SDLN of FTY720-treated mice (Figures S6A and S6B). Despite blocking lymphocyte trafficking to non-LOs, skin Treg depletion still led to increased numbers of skin Teffs and CD8+ T cells, and pro-inflammatory cytokine production by these cells at levels similar to those of non-FTY720 treated mice (Figures S6C–S6E). Additionally, these parameters were associated with increased folliculitis compared to control-treated skin (Figures S6F). These results suggest that autoreactive T cells present in skin are actively restrained by skin resident Tregs in the steady-state.

Skin Tregs are characterized by a heightened immunoregulatory gene signature

We next sought to determine the molecular mechanisms Tregs utilize to suppress HF-associated inflammation. Although several mechanisms of Treg-mediated immunosuppression are known(6), those relevant in peripheral tissues has been a long-standing question that has been hampered by limitations inherent to systemic Treg gene manipulation(26, 27). To identify differences in the global transcriptome and expression of immunosuppressive molecules between murine SDLN and skin Tregs, we performed single cell RNA sequencing (scRNAseq) of Tregs purified from these organs. Unsupervised stochastic clustering showed that Tregs in skin are transcriptionally heterogenous and largely differ from SDLN Tregs, although a few subsets in skin and SDLN demonstrated overlapping transcriptional signatures (Figures 3A–3C). Clusters 1–3, 8, and 9 were heavily represented by SDLN Tregs and were enriched for genes characteristic of circulating lymphocytes and those that reside in secondary LOs (*e.g., Ccr7* and *Sell*; Figure 3D). Conversely, clusters 4–7 were dominated by skin Tregs, which preferentially expressed genes involved in suppressive activity (*Gzmb*, *Ctla4*), tissue repair (*Areg*), survival (*Il1rl1*), and co-stimulation/activation (*Icos, Tnfrsf4, Tnfrsf9*), respectively. These results are congruent with recent transcriptional studies of murine Tregs that have shown increased activation states and repair programs in Tregs from non-LOs compared to LOs(28, 29). Notably, skin Tregs exhibited higher expression of genes involved in maintaining peripheral tolerance, including *Il10*, *Gitr*, and *Ctla4*, compared to those in SDLN (Figure 3E). When combining these and other relevant genes into an immunoregulatory gene score, we found that skin Tregs expressed this signature to a greater extent than their SDLN counterparts (Figures 3F and 3G). A closer examination in the context of cellular heterogeneity found that the highest expressors of this gene signature was present in clusters 7, 4, 10, 5, and 6, which are largely represented by skin Tregs (Figure 3H). Cluster 7 was of particular interest because it is characterized by activation markers (*Tnfrsf4*, *Tnfrsf9*, *Icos*) as well as the transcription factor *Batf*, which has been implicated as a regulator of Tregs in LOs destined for tissue trafficking and of tissue Treg stability(29, 30).

To compare the suppressive capacity of skin and LO Tregs, *in vitro* suppression assays showed that while Tregs purified from secondary LOs suppressed Teff in a dose-dependent manner, those from skin did not demonstrate a similar suppression curve (Figure S7A). However, we found that skin Tregs were reduced in number and had lower Ki-67 labeling compared to LO Tregs (Figure S7B–S7C), supporting that Tregs in non-LOs reflect a more terminally differentiated effector state(28, 29) with lower proliferative capacity (Figure S7D). We posit that the terminal differentiation state of skin Tregs may prevent optimal proliferation *in vitro*. Nonetheless, the expression of a heightened immunosuppressive

transcriptional module supports our observation that skin-resident Tregs actively suppress cutaneous inflammation in the steady-state.

CTLA-4 is not required by skin Tregs to suppress inflammation in the steady-state

CTLA-4 is an immunoglobulin superfamily member whose expression on Tregs maintains immune homeostasis by sequestering co-stimulatory molecules from antigen presenting cells (APCs), thus depriving effector T cells of optimal activation signals(31). scRNAseq showed *Ctla4* to be among the most highly enriched immunosuppressive molecules in skin compared to SDLN Tregs (Figure 3E). Interestingly, SDLN Tregs that express the highest levels of *Ctla4* were present in a cluster that had an overlapping transcriptional signature with a subset of skin Tregs (Figure 4A), suggesting the presence of Tregs in SDLN destined to traffic to skin and/or a subset of Tregs that have the propensity to recirculate after skin residency. Flow cytometry confirmed that CTLA-4 is more highly expressed by skin Tregs compared to SDLN Tregs (Figure 4B).

To directly explore the contribution of CTLA-4 on skin Tregs in restraining HF-associated inflammation, we crossed Foxp3-Cre$^{ERT2\text{-}GFP}$ mice to CTLA-4$^{fl/fl}$ mice to generate Foxp3-Cre$^{ERT2\text{-}GFP}$ × CTLA-4$^{fl/fl}$ mice (Foxp3$^{\Delta CTLA-4}$). Topical treatment of Foxp3$^{\Delta CTLA-4}$ mohawk mice for four weeks (Figure 4C) showed persistent deletion of CTLA-4 on skin-resident Tregs in 4OHT-treated compared to control-treated skin at a magnitude comparable to that of skin Tregs in Tamoxifen-treated mice (Figures 4D). Moreover, the frequency of CTLA-4-expressing Tregs in SDLN that drained 4OHT- versus control-treated skin was roughly equivalent compared to the near total loss of CTLA-4 on SDLN Tregs from Tamoxifen-treated mice (Figures 4D). This approach shows robust, specific, and localized deletion of CTLA-4 on skin Tregs and demonstrates efficacy of targeted gene deletion in a lymphocyte subset (*i.e.,* Tregs) in a single organ.

Despite significant loss of CTLA-4 on skin Tregs, the frequency and number of skin-resident Tregs was unperturbed (Figure 4E). Additionally, the number of skin CD8+ T cells and Teffs and pro-inflammatory cytokine production by these cells did not differ from contralateral control-treated skin (Figures 4F and 4G). Transendocytosis of co-stimulatory molecules (*e.g.* CD80 and CD86) from the plasma membrane of APCs by CTLA-4-expressing Tregs has been posited as a mechanism of immune suppression(31). However, loss of CTLA-4 on skin Tregs did not alter the level of CD80 and CD86 expression on skin DCs or macrophages nor did it markedly impact their expression of major histocompatibility class II (Figure 4H). Histologic examination demonstrated that skin Treg-specific CTLA-4 deletion did not result in HF-associated inflammation (Figure 4I). Taken together, these results indicate that despite preferential high expression by skin Tregs, CTLA-4 does not influence the activation state of skin APCs in the steady-state or impact effector T cell accumulation/activation in skin. This result is in contrast to prior studies demonstrating that CTLA-4 on Tregs is required to restrain autoimmunity(32, 33), suggesting that CTLA-4 is relatively dispensable for Treg-mediated cutaneous immune homeostasis in adult mice.

CD25 expression by skin Treg restrains hair follicle-associated inflammation

We next investigated the role of CD25, the high affinity subunit of the interleukin-2 (IL-2) receptor, which is encoded by *Il2ra*. CD25 induces and maintains Treg identity in the thymus and secondary LOs, respectively(34–36). Additionally, IL-2 has been shown to promote Treg accumulation in the small intestine(37). scRNAseq and flow cytometry showed that CD25 is highly expressed by both skin and SDLN Tregs at the mRNA and protein levels (Figures 5A and 5B). Flow cytometry of skin from IL-2-green fluorescent protein (GFP) reporter mice showed that while IL-2 is expressed most highly by innate lymphoid cells, Teffs, and CD8+ T cells, the former two subsets dominate the absolute pool of IL-2-expressing lymphocytes in skin (Figures 5C, 5D, and Figure S8), similar to the expression pattern seen in the small intestine(37). Tregs in secondary LOs highly express CD25 where it has been shown to sequester IL-2, thus depriving effector T cells of this activation/survival signal(34, 38). Indeed, constitutive loss of CD25 expression on Tregs precipitated fatal autoimmunity in mice(34). However, it is unknown whether Tregs in non-LOs rely on CD25 expression for their maintenance and/or whether they use this molecule to suppress inflammation in the steady-state.

To directly address these questions, we crossed Foxp3-Cre$^{ERT2\text{-}GFP}$ mice to CD25$^{fl/fl}$ mice to generate Foxp3-Cre$^{ERT2\text{-}GFP}$ × CD25$^{fl/fl}$ mice (Foxp3$^{\Delta CD25}$) and treated mohawk mice for 4 weeks with topical 4OHT or vehicle control (Figure 5E). Flow cytometry demonstrated that the frequency and expression level of CD25 on skin-resident Tregs was substantially decreased in 4OHT- compared to control-treated skin, while these parameters were not different in SDLN Tregs (Figures 5F). Loss of CD25 on skin Tregs did not affect their accumulation (Figure 5G) but was instead associated with increased numbers of skin-resident CD8+ T cells and Teffs (Figure 5H). This was likely due to increased proliferation of these cells as evidenced by increased Ki-67 expression (Figure 5I). Loss of CD25 on skin Tregs did not significantly alter the frequency of other skin lymphoid or myeloid subsets (Figure S4E). Furthermore, absence of CD25 on skin Tregs resulted in an increased number of pro-inflammatory cytokine-producing CD8+ T cells and Teffs (Figure 5J). IL-2 signaling maintains Treg identity in secondary LOs, in part by stabilizing Foxp3, the lineage-defining transcription factor of Tregs(34, 39, 40). Contrary to decreased Foxp3 expression observed in LO Tregs from mice undergoing systemic CD25 deletion on Tregs(34, 35), we found that skin-resident Tregs depleted of CD25 maintained Foxp3 expression at levels similar to that of their CD25-expressing counterparts from contralateral control-treated skin (Figure 5K).

IL-2 signaling in T cells results in phosphorylation of signal transducer and activator of transcription 5 (pSTAT5)(41). Increased pSTAT5 expression was observed in CD8+ T cells and Teffs from the skin of CD25-deficient Tregs, suggestive of increased bioavailable IL-2 (Figure 5L). To assess the functional consequence of heightened activation of effector T cells in the absence of CD25-expressing skin Tregs, tissue sections were examined for evidence of skin pathology, which showed increased folliculitis in skin of 4OHT-treated Foxp3$^{\Delta CD25}$ mice (Figure 5M). Since deletion of CD25 would not wholly abrogate IL-2 signaling in skin Tregs (expression of the low-affinity IL-2 receptor, *Il2rb* (CD122), would not be altered), we sought to determine if IL-2 production in skin has an impact on skin Treg biology. To address this question, we generated Ubiq-Cre^{ERT2} × IL-2$^{fl/fl}$ mice which have

the potential for *Il2* deletion in all cell types in skin under the influence of topical 4OHT. Treatment of these mice with this regimen demonstrated a slight but significant reduction in the number of skin Tregs without perturbing expression of Foxp3 (Figures 5N and 5O). Overall, these results demonstrate that unlike Tregs in LOs(34), skin-resident Tregs do not rely on CD25 or IL-2 to maintain lineage stability through expression of Foxp3, but rather, CD25 expression on skin Tregs restrains T cell-mediated HF-associated inflammation in a cell-extrinsic fashion.

Skin Tregs restrain autoimmune attack of hair follicle stem cells

Based on the appearance of T cell-mediated inflammation in Treg-depleted skin (Figure 2), we posited that skin Tregs can suppress autoreactive T cells specific for HF-derived antigens. We previously showed that a subset of skin Tregs localize to the bulge region of HFs(14). This microanatomic HF niche contains epithelial stem cells, characterized by expression of leucine rich repeat containing G protein-coupled receptor 5 (Lgr5), that enable hair growth(42). Since maintenance of stem cell niches is important to sustaining life by promoting tissue regeneration, we hypothesized that a critical function of Tregs is to protect HF stem cells (HFSCs) from autoimmune attack. Thus, we crossed Lgr5-Cre$^{ERT2\text{-}GFP}$ mice to Rosa26-*LSL*-OVA-GFP(43) mice to generate mice in which a neo-antigen, chicken ovalbumin (OVA), is expressed in Lgr5+ HFSCs upon Tamoxifen administration (Lgr5^{iOVA} mice). To address whether skin Tregs restrain self-reactive CD8+ T cells from attacking HFSCs, Lgr5^{iOVA} mice were treated with Tamoxifen to induce OVA expression in HFSCs, and thereafter, chimeric mice were generated in which donor Foxp3^{iDTA} bone marrow was transferred to irradiated Tamoxifen-treated, OVA-expressing Lgr5^{iOVA} recipients (Figure 6A). After bone marrow reconstitution, congenically mismatched CD8+ T cells expressing a transgenic T cell receptor specific for an OVA-derived epitope (CD45.1+ OT-I T cells) were transferred intravenously into OVA-expressing Foxp3^{iDTA} → Lgr5^{iOVA} chimeric mice (CD45.2+). One week after transfer, chimeric mice were shaved in a mohawk configuration and treated topically with 4OHT or vehicle control to deplete Tregs in skin. Importantly, topical 4OHT application did not lead to increased OVA-GFP expression in HFSCs, which was already at maximal expression after initial Tamoxifen treatment (Figure 6B). Increased OT-I T cell accumulation, proliferation, CD25 expression, and pro-inflammatory cytokine production were observed in Treg-depleted skin relative to contralateral control-treated skin (Figures 6C–6G). Heightened activation of OT-I T cells in Treg-depleted skin was associated with decreased numbers and diminished Lgr5-driven GFP expression in HFSCs, suggesting that elimination or damage to OVA-GFP+ HFSCs had occurred (Figures 6H–6J). Histology showed that increased OT-I T cell activation in Treg-depleted skin was associated with heightened lymphocytic inflammation with a striking selectivity for the lower reticular dermis (Figure 6K and 6L (left panel)). This contrasts with the inflammation seen along the full length of the hair follicle when skin Tregs were depleted in a polyclonal setting (Figure 2I), providing support for antigen-specific accumulation of OT-I T cells to the HF bulge in Foxp3^{iDTA} → Lgr5^{iOVA} chimeric mice. Additionally, greater numbers of lymphocytes within bulge epithelium, and increased apoptotic bulge keratinocytes were observed in Treg-depleted skin (Figure 6L (middle and right panels)).

Since we observed that CD25 on skin Tregs restrains CD8+ T cell activation (Figure 5) and skin OT-I T cells upregulate CD25 in response to skin-specific Treg-depletion in $Foxp3^{iDTA} \rightarrow Lgr5^{iOVA}$ chimeric mice (Figure 6F), we hypothesized that IL-2 deprivation by CD25-expressing Tregs may restrain OT-I T cell accumulation and HFSC damage. To test this, we generated chimeric mice using the same methods as above but using donor $Foxp3^{\Delta CD25}$ bone marrow instead. Following OT-I transfer and topical 4OHT treatment, deletion of CD25 on skin Tregs was associated with increased epithelial OT-I T cell accumulation, decreased expression of GFP by Lgr5+ HFSCs, and increased foci of HF bulge inflammation (Figures 6M–6P). Collectively, these results establish an immunoregulatory role for skin Tregs in protecting HFSCs from attack by autoreactive CD8+ T cells.

Human autoimmune alopecia is characterized by heightened IL-2/STAT5 signaling around hair follicles

The results from our murine experiments implicated a model in which CD25 acts to restrain autoreactive CD8+ T cell activation in skin, likely by sequestering IL-2, which prevents excessive damage to HFSCs undergoing autoimmune attack. Although significant perifollicular fibrosis was not observed in $Foxp3^{iDTA} \rightarrow Lgr5^{iOVA}$ chimeric mouse experiments, the presence of lymphocyte-mediated attack of HFSCs in the latter model (Figure 6J–K) recapitulates certain histopathologic features of human scarring alopecia (SA) thought to be mediated by CD8+ T cells(44). In SA, autoreactive T cells target HFSCs leading to perifollicular concentric fibrosis and irreversible hair loss. To directly investigate if increased IL-2/STAT5 signaling is present in the relevant pathologic microanatomic regions of disease in SA, namely in the stroma around HFs, we performed spatial transcriptomics on a tissue microarray (TMA) composed of four cores of formalin-fixed paraffin-embedded skin tissue from two patients with SA and two healthy controls (Figures S9A and S9B; Table S1). Unsupervised stochastic clustering identified thirteen distinct clusters that largely segregated according to the tissue of origin (Figures 7C, S9C and S9D) as well as by microanatomic regions within each sample (Figure S9E). The differences in transcriptional profile between the two SA samples may be attributable to the varying degrees of disease severity with SA #2 demonstrating a greater degree of inflammation and fibrosis than SA #1, differences in the subtype of SA, and/or varying treatments the patients received. Since the histopathological hallmark of SA is perifollicular lymphocytic infiltrates leading to fibrosis, we interrogated these areas in SA and corresponding regions in the healthy scalp skin for evidence of IL-2 signaling (Figure 7A). We found an enhancement of an *IL-2/STAT5* signaling gene signature in the perifollicular stroma of SA compared to healthy skin that partially overlapped with CD8 T cell and Treg gene signatures (Figures 7B and 7D). When comprehensively evaluating the stromal microanatomy, it was apparent that the *IL-2/STAT5* pathway gene signature, as well as the CD8+ T cell and Treg signatures, were most prominent in the regions of stroma surrounding HFs in SA (Figures 7D–7E). Immunohistochemical staining for CD8 and CD4/Foxp3 confirmed increased infiltrates of CD8+ T cells, Teffs, and Tregs in biopsies of SA compared to healthy skin (Figures S9F–S9H).

To determine if an enhanced *IL-2/STAT5* gene signaling signature was generalizable to other forms of lymphocyte-mediated alopecia, spatial transcriptomics was performed on a TMA constructed using alopecia areata (AA) patient biopsies (Figure S10A). AA is a form of non-scarring alopecia in which the hair follicle bulb is infiltrated by T cells causing hair follicles to prematurely involute. Unsupervised clustering identified distinct transcriptional gene signatures corresponding to different microanatomic regions in AA (Figures S10B–S10D). Analysis of the *IL-2/STAT5* gene signaling signature revealed an enhancement in the inflamed stroma adjacent to the hair follicle bulb that overlapped with CD8 and Treg gene signatures (Figures 7F–7J. Similar to SA, biopsies of AA also demonstrated increases in CD8+ T cells, Teff, and Treg infiltration in perifollicular regions (Figure S10E–S10G). Collectively, these data suggest that an IL-2 signaling-CD8+ T cell-Teff-Treg circuit is active in human lymphocyte-mediated alopecia.

Discussion

This study demonstrates a tissue-specific technique to ablate Tregs and selectively delete genes in these cells, helping to resolve a fundamental question of whether Tregs exert immunosuppressive functions in non-LOs. We demonstrate that skin-resident Tregs curtail cutaneous inflammation in the steady-state similar to a phenotype that arises when they are defective in trafficking to skin(18). This inflammatory phenotype is not secondary to disrupted barrier function since we previously showed that systemic loss of Tregs does not perturb skin integrity in the steady-state(22). These prior studies showed that systemic Treg depletion does not result in significant skin inflammation(14, 22), in contrast to the results of skin-specific Treg depletion observed in the current study (Figure 2), which is likely due to the acute manner of deletion (<7 days) in the former compared to chronic skin Treg depletion regimen in the latter.

Cutaneous inflammation observed when skin Tregs are depleted is likely directed against both self-antigen and commensal microbes. Intriguingly, organism-wide autoimmunity is maintained in mice systemically depleted of Tregs under germ-free conditions(45), and no differences in CD8+ T cell or Teff number are observed in the skin of germ-free mice(46), suggesting that much of the cutaneous inflammatory response when skin Tregs are depleted may be attributable to autoreactive T cells. Despite significant increases in effector T cell activation upon skin Treg depletion, the inflammatory pathology seen on microscopic examination was somewhat moderate (Figures 2I and 2J) as compared to more prominent inflammatory phenotype observed in mice that undergo prolonged complete systemic Treg ablation(7). This was not unexpected since a constraint of the $Foxp3^{iDTA}$ mouse strain used in this study was that an incomplete, ~50% reduction in skin Tregs could be achieved. We postulate that if Tregs were entirely depleted in skin, a more fulminant inflammatory phenotype would be observed. Nonetheless, this technique was used to uncover a previously undescribed role for Tregs in protecting HFSCs that, when disrupted, leads to localized autoimmune hair damage in a manner that resembles human alopecia (47–49). In contrast to prior studies that demonstrated a role for Tregs in promoting the differentiation and migration of HFSCs during hair regrowth(14) or epidermal injury(22), we now show that Tregs in skin also mediate a more classical role of immunoregulation in this tissue. Our data adds to the emerging body of evidence that Tregs in skin are strategically positioned around

HFs to dually protect HFSCs from autoimmunity as well as promote tissue regeneration(14, 22).

We found that expression of CD25, but not CTLA-4, on skin-resident Tregs was necessary to partially restrain CD8+ T cell-mediated cutaneous inflammation in the steady-state. This suggests that co-stimulation blockade is not a dominant mechanism of Treg-mediated immunosuppression in non-inflamed adult skin, which may be explained by the relative immaturity of tissue-resident APCs during homeostasis compared to those migrating to LOs(50). Notably, the magnitude of T cell activation and folliculitis was less when CD25 was deleted on skin Tregs compared to when these cells were depleted (Figure 2 vs Figure 5), which is not unexpected, as Tregs utilize multiple functionally redundant mechanisms of immune regulation(51). Our results suggest that a major function of CD25 expression on skin-resident Tregs is to limit bioavailable IL-2 to prevent aberrant T cell activation, analogous to its function in secondary LOs(34, 38). However, CD25 does not act to maintain skin-resident Treg identity as it does in Tregs in LOs(34–36). This is probably due to stabilization of Foxp3 protein expression of LO-resident Tregs through epigenetic modification of the *Foxp3* locus before Tregs traffic to non-LOs(39). We also show that the predominant IL-2-producing cells in the skin are Teffs and ILCs, and a subset of these cells have been shown accumulate around HFs(52, 53). Therefore, localization of skin Tregs to this microanatomic niche suggests that cellular interactions between Tregs and IL-2-producing lymphocyte subsets may be necessary to maintain cutaneous immune tolerance. Ultimately, our results indicate that expression of immunomodulatory molecules on Tregs have different functional relevance depending on anatomic site, which is an important consideration for therapeutics that have the potential to modulate Treg biology.

The observation of folliculitis in the setting of skin Treg depletion and CD25 deletion on Tregs suggests that a subset of these cells have specificity to self-antigens expressed by the HF. While mostly speculative, one explanation for preferential protection of HFs by skin Tregs is that HFs are composed of distinct keratinocyte subsets each expressing numerous genes largely restricted to skin(54). Indeed, almost half of human cytokeratin genes have expression restricted to the HF(55). Such a high abundance and diversity of HF-specific antigens suggests that central tolerance may be insufficient to delete the full complement of skin-specific, self-reactive T cells. Interestingly, Aire-deficient mice fail to exhibit autoimmunity in skin(56). Furthermore, some skin-specific antigens are not expressed in the thymus at levels that engender negative selection, thus, allowing self-reactive clones to enter the periphery(57). Teleologically, the positioning of a subset of Tregs around HFs may act to blunt autoimmune attack by self-reactive T cells. Further studies will be necessary to decisively elucidate the self-antigen specificity of Tregs that protect HFSCs and HF epithelium.

We found an elevated IL-2 signaling gene signature in SA, suggesting that dysregulation of this pathway may contribute to the pathogenesis of this disease. Indeed, IL-2 has been shown to potentiate memory CD8+ T cell responses in models of chronic antigen stimulation(58) analogous to the situation encountered in autoimmune disease. Additionally, *IL2RA* (CD25) and *IL2* are known to be susceptibility genes for AA(59), providing evidence that CD25 on Tregs in humans may be necessary to blunt HF-

associated autoinflammation. We speculate that evolutionarily conserved mechanisms of Treg immunoregulation in skin (e.g., CD25) may be required to tolerate the development of microanatomic structures of great cellular and antigenic complexity.

The technique of skin-specific Treg manipulation presented herein has long been a ‘wish list’ item of tissue Treg investigation(60). This approach offers several advantages over traditional methods of Treg modulation (e.g. Foxp3-Cre mice or Foxp3-Cre$^{ERT2\text{-}GFP}$ mice + systemic Tamoxifen administration), which have remained the dominant methodology to study tissue Treg biology despite potentially affecting these cells throughout development and in all tissue compartments. These latter methods may also potentially lead to more pronounced phenotypes than if experiments were conducted in a manner that only alters Tregs in a tissue-specific context. Tissue-specific Treg modulation can be conducive to intra-animal (paired) comparisons since an internal control (e.g., control-treated skin) can be used, which can potentially reduce the number of mice mice needed for a given experiment. While intra-animal comparisons allow more robust statistical analyses by mitigating variation and noise between different animals (inter-animal comparisons), it may lend more modest differences in inflammatory parameters and pathology. Furthermore, this technique could be extended to study tissue-specific immune functions in other organs that are amenable to topical application (e.g., conjunctiva) and surgical techniques could potentially be adapted to selectively study the immune system in visceral organs. Overall, more definitive conclusions of tissue Treg biology can be made by experimentation that modulates Tregs in an organ-specific fashion.

Fundamentally, our data supports a model in which immunologic tolerance is not only confined to LOs but is also operant in non-LOs, congruent with the emerging concept that non-LOs can act as autonomous decentralized sites of cellular immunity(61). Ultimately, Tregs in these tissues may represent a final safeguard against autoreactive T cells that manage to evade tolerance in LOs.

Materials and methods

Study design

The aim of this study was to functionally manipulate Treg in skin to determine whether they have immunoregulatory functions. Thus, we developed a topical application method using 4OHT to genetically modulate skin Tregs. This allowed for pairwise comparisons of control-treated and contralateral 4OHT-treated skin in most experiments. Short- and long-term experiments in which skin Tregs were fluorescently-labeled, depleted, or had genes deleted were undertaken. Pathologic signs of inflammation were assessed using H&E sections of mouse skin and scored in a blinded fashion. Immunologic parameters of inflammation were evaluated by flow cytometry of single cell suspensions of skin and lymph node tissues. Cohort size was designed to be sufficient to enable accurate determination of statistical significance. Mice were assigned to treatment or control groups randomly.

Animals

All animals were bred and maintained in a specific pathogen free mouse facility in accordance with the Laboratory Animal Resource Center and Institutional Animal Care and Use Committee of the University of California San Francisco (UCSF). Mice were socially housed under a 12-hour day/night cycle. Littermate controls were used for all experiments, and animals of both sexes were included. Sex, parental cage, and weaning cage were randomized among experimental groups. Strains used in this study include Foxp3-Cre$^{ERT2\text{-}GFP}$ (Foxp3$^{tm9(EGFP/cre/ERT2)Ayr}$); FoxP3^{DTR} (Foxp3$^{tm3(DTR\text{-}GFP)Ayr}$); Foxp3-GFP (Foxp3^{tm2Tch}); Rosa26^{tdTomato} (Gt(ROSA)26Sor$^{tm14(CAG\text{-}tdTomato)Hze}$); Rosa26^{iDTA} (Gt(ROSA)26Sor$^{tm1(DTA)Mrc}$), Lgr5-Cre^{ERT2} (Lgr5$^{tm1(Cre/ERT2)Cle}$), CD25$^{fl/fl}$ (Il2ra$^{tm1c(EUCOMM)Wtsi}$), OT-I CD45.1 (kindly provided by Dr. Matthew Krummel), CTLA-4$^{fl/fl}$ (kindly provided by Dr. Arlene H. Sharpe), IL-2^{GFP} (kindly provided by Dr. Casey T. Weaver), and Rosa26^{OVA} (kindly provided by Dr. Angelika Stoecklinger).

Administration of Tamoxifen, 4OHT, diphtheria toxin, and FTY720

Tamoxifen (Sigma-Aldrich) was dissolved in corn oil (Sigma-Aldrich) at 37°C by shaking overnight. For Cre recombinase induction in Foxp3^{iDTA}, Foxp3$^{\Delta CTLA-4}$, and Foxp3$^{\Delta CD25}$ mice, Tamoxifen was administered intraperitoneally at a dose of 100 mg/kg every three days for 4 weeks and 2 weeks, respectively. In experiments using Lgr5^{iOVA} mice, Cre recombinase was activated via intraperitoneal injection of Tamoxifen on days −6 and −5. In experiments using topical 4OHT (Sigma-Aldrich), 5 mg of 4OHT was dissolved in 10 ml of acetone (Sigma-Aldrich) to generate a stock concentration of 500 μg/ml. 4OHT was further diluted with acetone to generate working concentrations of 100 μg/ml (1:5 dilution), 50 μg/ml (1:10 dilution), or 20 μg/ml (1:25 dilution). 100 μl of 4OHT/acetone at a working concentration was then applied to anesthetized mice in a dropwise manner to one side of exposed dorsal back skin of mice shaved in a mohawk configuration to cover the entire shaved skin surface (no depilation is performed). Acetone alone was applied in the same manner to the contralateral side of shaved dorsal back skin. Given the relatively high vapor pressure of acetone, there is no residual liquid to remove from the skin and the mice are returned to their cage. This procedure is repeated for 5 consecutive days for some experiments and then applied every two to three days for 2–4 weeks in extended experiments. Foxp3^{tdTomato} mice, 4OHT was used at a concentration of 20 μg/ml. In experiments involving, Foxp3$^{\Delta CTLA-4}$ and Foxp3$^{\Delta CD25}$ mice, 4OHT was used at a concentration of 50 μg/ml. In experiments involving Foxp3^{iDTA} mice, 4OHT was used at a concentration of 100 μg/ml. In experiments involving FTY720 (Selleck Chemicals) treatment, 25 μg of FTY720 in 100 μl of PBS was injected intraperitoneally every three days for 4 weeks until tissues were harvested.

Tissue Processing

After euthanasia, whole back skin was shaved and dissected. Any remaining scapular or inguinal fat was removed, and the remaining tissue was weighed, finely minced with scissors, placed in a 50 mL conical containing 3 mL of digestion media (2 mg/mL collagenase XI, 0.5 mg/mL hyaluronidase, 0.1 mg/mL DNase in RPMI with 10% calf

serum, 1% HEPES, 1% non-essential amino acids, 1% GlutaMAX, and 1% penicillin-streptomycin), and digested in a bacterial shaker for 45 minutes at 37°C and 225 rpm. Digestion was then quenched with 10 mL of cold RPMI and samples were vortexed for 10 seconds and strained through 100 μm strainers. The resulting single cell suspension was then plated in 96-well plates for staining. For lymph node samples, axillary, brachial, and inguinal lymph nodes ("SDLN", collectively) were dissected and mashed through a 40 μm filter with a 5 mL syringe plunger into cold media. For cutaneous epithelial cell preparations for flow cytometric analysis, 2.25 cm^2 of back skin was harvested and defatted mechanically using forceps. Skin was placed dermis side down in a well of a 12-well plate with 1 mL of Thermolysin (0.25 mg/ml; Sigma) and placed in a 37°C incubator for 1 hour. Skin epithelium was gently disassociated from the underlying dermis in a petri dish containing 1 mL RPMI/HEPES/P-S/FCS media using forceps and minced with scissors. Media containing epithelial fragments was pipetted up and down using a P1000 pipette 20 times before filtering through 100 μm strainers. Cells were counted and stained for flow cytometry.

Flow Cytometry

Single-cell suspensions were pelleted and resuspended in PBS with 2% FBS containing fluorophore-conjugated antibodies listed in the key resources table (Table 2). Cells were initially stained with antibodies targeting cell surface proteins and Ghost 510 viability dye (Tonbo Biosciences) for 30 min. For intracellular staining, cells were then fixed and permeabilized using the Cytofix/Cytoperm kit (BD Biosciences). For experiments involving intracellular cytokine staining (ICS), single cell suspensions were plated at 4×10^6 cells/well in a 96-well round bottom plate, resuspended in 1X cell stimulation cocktail (Tonbo Biosciences), and incubated at 37°C for 4 hours before antibody staining. Samples were run for analysis on a BD Fortessa or sorted on a BD FACS Aria2.

For all cell types, initial forward scatter vs. side-scatter gates were carefully adjusted by backgating on live CD45+ and/or live CD45− populations to include all cells and exclude debris. Strict dead cell and doublet exclusion was performed prior to gating for immune cells (CD45+) and/or epithelial cells (CD45−). αβT cells were gated as CD45+ TCRβ+ and subsetted into Teffs (CD4+FoxP3−), Tregs (CD4+FoxP3+), CD8 T cells (CD8+). Non-αβT cells were gated as CD45+ CD3+ γδ+ and subsetted into dermal γδ T cells (TCRβ− $CD3^{mid}$) and dendritic epidermal T cells (DETCs, TCRβ− $CD3^{hi}$). GFP fluorescent protein expression in $Foxp3^{CreERT2\text{-}GFP}$ mice and IL-2-GFP reporter mice was used to report Foxp3 expression and IL-2 expression, respectively. Macrophages (CD64+ CD11b+ CD11c−) and dendritic cells (CD64-MHCII+CD11c+) were gated after excluding T cells, eosinophils (CD45+ Ly6G− CD11b+ Siglec-F+), and neutrophils (CD45+ Ly6G+ MHC II−). HFSCs in skin epithelial preparations were gated as CD45− Sca-1- $EpCAM^{int}$ CD34+. GFP fluorescent protein expression in $Lgr5^{iOVA}$ mice was used as a proxy for OVA-GFP fusion protein expression. Cell numbers were calculated by quantifying cell numbers on a NucleoCounter (ChemoMetec) prior to staining.

Immunofluorescence microscopy

For immunofluorescent tissue staining, shaved back skin strips, lung lobes, colon segments, inguinal lymph nodes, mesenteric lymph nodes, and spleens from Foxp3^{tDtomato} mice were fixed in 2% paraformaldehyde on a rocker at room temperature for 4 hours. After washing in PBS, tissues were embedded in optical cutting temperature compound (OCT) and flash-frozen in isopentane (Sigma) cooled with dry ice. 10 μm sections were cut on a cryostat (ThermoFisher Cryostar NX50) onto SuperFrost Plus slides. Tissue sections were air-dried for one hour, washed in PBS, and mounted in ProLong Gold antifade reagent with DAPI (ThermoFisher). Tissues were imaged on a Keyence Fluorescence BZ-X810 microscope. The number of tdTomato+ Tregs was quantified per 200x high power field (HFP) across 6 randomly HFPs per tissue section.

Single-cell RNA sequencing

Skin Tregs were isolated from four Foxp3-Cre$^{ERT2\text{-}GFP}$ adult female mice. Back skin was harvested, enzymatically digested, and processed as detailed above. SDLN Tregs were prepared by harvesting pooled inguinal, brachial, and axillary LNs from two Foxp3-GFP reporter adult female mice and were processed as detailed above. Skin and SDLN Tregs (CD45+ TCRβ+ CD8− CD4+ GFP+) were sort purified on a BD FACSAriaII using a 100μm nozzle and sorted into RPMI + 10% FBS.

Samples were run on separate lanes of a 10X Chromium chip with 3’ v2 chemistry (10X Genomics) following manufacturer instructions by the UCSF Institute for Human Genetics Sequencing Core. Libraries were sequenced on an Illumina NovaSeq 6000. Fastq files were aligned to the mm10 reference genome and barcode matrices were generated using Cellranger 2.1. For skin Tregs, 2,058 median unique molecular identifiers (UMIs; transcripts) per cell, and 1035 median genes per cell were sequenced to 91.6% sequencing saturation with 88,229 mean reads per cell. For SDLN Tregs, For SDLN Tregs, 3,021 median UMIs per cells, and 1,155 median genes per cell were sequenced to 88.4% sequencing saturation with 60,753 means reads per cell.

Spatial Transcriptomics

The procurement of archived patient formalin-fixed paraffin-embedded tissue was approved by the human research ethics committee of UCSF (21–33678) and was conducted according to the Declaration of Helsinki and a waiver of informed consent was granted as no study procedures were performed. Two scarring areata patient biopsy samples and two healthy human scalp skin samples were retrieved from the diagnostic and consultation archives of the UCSF Dermatopathology Service. Additionally, two alopecia areata patient biopsy samples were retrieved from the diagnostic and consultation archives of the UCSF Dermatopathology Service. H&E slides were reviewed by an expert dermatopathologist (J.N.C.) to confirm the diagnosis. FFPE tissue blocks for each sample were retrieved. A tissue microarray (TMA) was constructed by using an automated TMA machine to punch a 2-millimeter core from each tissue block in the region of interest and place the resulting tissue core into a separate paraffin block, such that the four cores were arrayed in a 2 × 2 grid.

Visium spatial gene expression slides for human FFPE and reagents kits were used according to manufacturer instructions (10X Genomics). Initial tissue sections confirmed a DV200 score of over 5. Next, a 5 μm section from the TMA was cut using standard microtomy and placed in one capture area (6.5 × 6.5 mm^2) of a specialized 10x Visium slide. Each capture area contains ~5,000 barcoded spots that are 55 mm in diameter (100 mm center to center between spots) providing an average resolution of 1 to 10 cells. The tissue section was then prepared according to the recommended protocols (tissue preparation guide CG000408). H&E image preparation was performed according to protocol (deparaffinization, H&E staining, Imaging and decrosslinking, CG000408). Spatial gene expression assay was performed according to the protocol CG000407. Libraries were prepared with Truseq Illumina libraries and sequenced on a NextSeq (Illumina). Sequencing was performed with the recommended protocol (read 1: 28 cycles; i7 index read: 10 cycles; i5 index read: 10 cycles; and read 2: 50 cycles), yielding 142,524,366 sequencing reads for the scarring alopecia TMA sample and 121,110,575 sequencing reads for the alopecia areata TMA sample. For the scarring alopecia TMA sample, 1,420 spots were identified as being under tissue were sequenced with a mean read per spot of 100,369 and 4,382 median genes per spot. For the alopecia areata TMA sample, 1,211 spots were identified as being under tissue were sequenced with a mean read per spot of 100,009 and 3,753 median genes per spot.

Quantification and statistical analysis

Statistical analyses were performed using Prism software package 9.0 (GraphPad). p values were calculated using two-tailed unpaired or paired Student's *t*-test and one- or two-way ANOVA and as indicated in the Figure Captions. Apart from scRNAseq and spatial transcriptomics, all experiments were repeated 2–3 times, and all data points represent individual biological replicates.

Supplementary Material

Refer to Web version on PubMed Central for supplementary material.

Acknowledgments:

We thank the staff of the UCSF Laboratory Animal Resource Center, Parnassus Flow Cytometry Core, the UCSF Institute for Human Genetics (single cell RNA sequencing), and the UCSF Dermatopathology Service (histology) for research support.

Funding:

The Parnassus Flow Cytometry Core (RRID:SCR_018206) is supported in part by NIH P30 DK063720 and by the NIH S10 Instrumentation Grant 1S10OD021822–01. This work was primarily supported by NIH NIAMS grants: (R01AR077553 and R01AR071944) to M.D.R. (T32AR007175–44, K08AR079596, and Dermatology Foundation P0549880 [CA-0175044]) to J.N.C. NIH P01AI56299 to A.S.

Data and materials availability:

scRNAseq data are available on GEO with accession numbers GSE175746 and GSE136160. Spatial transcriptomic data are available on GEO with accession number GSE227632. All correspondence and requests for materials and coding scripts can be made to the

corresponding author M.D.R. All other data needed to evaluate the conclusions in this study are present in the paper or the Supplementary Materials.

References

1. Kyewski B, Klein L, A Central Role for Central Tolerance. Annual Review of Immunology. 24, 571–606 (2006).
2. Anderson MS, Venanzi ES, Klein L, Chen Z, Berzins SP, Turley SJ, von Boehmer H, Bronson R, Dierich A, Benoist C, Mathis D, Projection of an immunological self shadow within the thymus by the aire protein. Science. 298, 1395–1401 (2002). [PubMed: 12376594]
3. Gallegos AM, Bevan MJ, Central tolerance: good but imperfect. Immunol Rev. 209, 290–296 (2006). [PubMed: 16448550]
4. Mueller DL, Mechanisms maintaining peripheral tolerance. Nat Immunol. 11, 21–27 (2010). [PubMed: 20016506]
5. Krishnamurty AT, Turley SJ, Lymph node stromal cells: cartographers of the immune system. Nat Immunol. 21, 369–380 (2020). [PubMed: 32205888]
6. Josefowicz SZ, Lu L-F, Rudensky AY, Regulatory T cells: mechanisms of differentiation and function. Annu Rev Immunol. 30, 531–564 (2012). [PubMed: 22224781]
7. Kim JM, Rasmussen JP, Rudensky AY, Regulatory T cells prevent catastrophic autoimmunity throughout the lifespan of mice. Nat Immunol. 8, 191–197 (2007). [PubMed: 17136045]
8. Lahl K, Loddenkemper C, Drouin C, Freyer J, Arnason J, Eberl G, Hamann A, Wagner H, Huehn J, Sparwasser T, Selective depletion of Foxp3+ regulatory T cells induces a scurfy-like disease. J Exp Med. 204, 57–63 (2007). [PubMed: 17200412]
9. Rosenblum MD, Gratz IK, Paw JS, Lee K, Marshak-Rothstein A, Abbas AK, Response to self antigen imprints regulatory memory in tissues. Nature. 480, 538–542 (2011). [PubMed: 22121024]
10. Sanchez Rodriguez R, Pauli ML, Neuhaus IM, Yu SS, Arron ST, Harris HW, Yang SH-Y, Anthony BA, Sverdrup FM, Krow-Lucal E, MacKenzie TC, Johnson DS, Meyer EH, Löhr A, Hsu A, Koo J, Liao W, Gupta R, Debbaneh MG, Butler D, Huynh M, Levin EC, Leon A, Hoffman WY, McGrath MH, Alvarado MD, Ludwig CH, Truong H-A, Maurano MM, Gratz IK, Abbas AK, Rosenblum MD, Memory regulatory T cells reside in human skin. J. Clin. Invest. 124, 1027–1036 (2014). [PubMed: 24509084]
11. Bennett CL, Christie J, Ramsdell F, Brunkow ME, Ferguson PJ, Whitesell L, Kelly TE, Saulsbury FT, Chance PF, Ochs HD, The immune dysregulation, polyendocrinopathy, enteropathy, X-linked syndrome (IPEX) is caused by mutations of FOXP3. Nat Genet. 27, 20–21 (2001). [PubMed: 11137993]
12. Nieves DS, Phipps RP, Pollock SJ, Ochs HD, Zhu Q, Scott GA, Ryan CK, Kobayashi I, Rossi TM, Goldsmith LA, Dermatologic and immunologic findings in the immune dysregulation, polyendocrinopathy, enteropathy, X-linked syndrome. Arch Dermatol. 140, 466–472 (2004). [PubMed: 15096376]
13. Choi YM, Wang YT, Geng B, Garcia-Lloret M, Smart CN, Lichenoid Dermatitis in an Adult with Immune Dysregulation, Polyendocrinopathy, Enteropathy, X-Linked (IPEX) Syndrome. Skinmed. 15, 231–234 (2017). [PubMed: 28705291]
14. Ali N, Zirak B, Rodriguez RS, Pauli ML, Truong H-A, Lai K, Ahn R, Corbin K, Lowe MM, Scharschmidt TC, Taravati K, Tan MR, Ricardo-Gonzalez RR, Nosbaum A, Bertolini M, Liao W, Nestle FO, Paus R, Cotsarelis G, Abbas AK, Rosenblum MD, Regulatory T Cells in Skin Facilitate Epithelial Stem Cell Differentiation. Cell. 169, 1119–1129.e11 (2017). [PubMed: 28552347]
15. Rubtsov YP, Niec RE, Josefowicz S, Li L, Darce J, Mathis D, Benoist C, Rudensky AY, Stability of the regulatory T cell lineage in vivo. Science. 329, 1667–1671 (2010). [PubMed: 20929851]
16. Rubtsov YP, Rasmussen JP, Chi EY, Fontenot J, Castelli L, Ye X, Treuting P, Siewe L, Roers A, Henderson WR, Muller W, Rudensky AY, Regulatory T cell-derived interleukin-10 limits inflammation at environmental interfaces. Immunity. 28, 546–558 (2008). [PubMed: 18387831]

17. Zhou X, Jeker LT, Fife BT, Zhu S, Anderson MS, McManus MT, Bluestone JA, Selective miRNA disruption in T reg cells leads to uncontrolled autoimmunity. J Exp Med. 205, 1983–1991 (2008). [PubMed: 18725525]

18. Dudda JC, Perdue N, Bachtanian E, Campbell DJ, Foxp3+ regulatory T cells maintain immune homeostasis in the skin. J. Exp. Med. 205, 1559–1565 (2008). [PubMed: 18573908]

19. Sather BD, Treuting P, Perdue N, Miazgowicz M, Fontenot JD, Rudensky AY, Campbell DJ, Altering the distribution of Foxp3+ regulatory T cells results in tissue-specific inflammatory disease. Journal of Experimental Medicine. 204, 1335–1347 (2007). [PubMed: 17548521]

20. Lim CK, Yuan ZX, Lamb JH, White IN, De Matteis F, Smith LL, A comparative study of tamoxifen metabolism in female rat, mouse and human liver microsomes. Carcinogenesis. 15, 589–593 (1994). [PubMed: 8149466]

21. Gregorio J, Meller S, Conrad C, Di Nardo A, Homey B, Lauerma A, Arai N, Gallo RL, Digiovanni J, Gilliet M, Plasmacytoid dendritic cells sense skin injury and promote wound healing through type I interferons. J Exp Med. 207, 2921–2930 (2010). [PubMed: 21115688]

22. Mathur AN, Zirak B, Boothby IC, Tan M, Cohen JN, Mauro TM, Mehta P, Lowe MM, Abbas AK, Ali N, Rosenblum MD, Treg-Cell Control of a CXCL5-IL-17 Inflammatory Axis Promotes Hair-Follicle-Stem-Cell Differentiation During Skin-Barrier Repair. Immunity. 50, 655–667.e4 (2019). [PubMed: 30893588]

23. Seneschal J, Clark RA, Gehad A, Baecher-Allan CM, Kupper TS, Human epidermal Langerhans cells maintain immune homeostasis in skin by activating skin resident regulatory T cells. Immunity. 36, 873–884 (2012). [PubMed: 22560445]

24. Ali N, Zirak B, Truong H-A, Maurano MM, Gratz IK, Abbas AK, Rosenblum MD, Skin-Resident T Cells Drive Dermal Dendritic Cell Migration in Response to Tissue Self-Antigen. J Immunol. 200, 3100–3108 (2018). [PubMed: 29563179]

25. Jung SR, Suprunenko T, Ashhurst TM, King NJC, Hofer MJ, Collateral Damage: What Effect Does Anti-CD4 and Anti-CD8α Antibody-Mediated Depletion Have on Leukocyte Populations? J Immunol. 201, 2176–2186 (2018). [PubMed: 30143586]

26. Panduro M, Benoist C, Mathis D, Tissue Tregs. Annu Rev Immunol. 34, 609–633 (2016). [PubMed: 27168246]

27. Lucca LE, Dominguez-Villar M, Modulation of regulatory T cell function and stability by co-inhibitory receptors. Nat Rev Immunol. 20, 680–693 (2020). [PubMed: 32269380]

28. Miragaia RJ, Gomes T, Chomka A, Jardine L, Riedel A, Hegazy AN, Whibley N, Tucci A, Chen X, Lindeman I, Emerton G, Krausgruber T, Shields J, Haniffa M, Powrie F, Teichmann SA, Single-Cell Transcriptomics of Regulatory T Cells Reveals Trajectories of Tissue Adaptation. Immunity. 50, 493–504.e7 (2019). [PubMed: 30737144]

29. Delacher M, Imbusch CD, Hotz-Wagenblatt A, Mallm J-P, Bauer K, Simon M, Riegel D, Rendeiro AF, Bittner S, Sanderink L, Pant A, Schmidleithner L, Braband KL, Echtenachter B, Fischer A, Giunchiglia V, Hoffmann P, Edinger M, Bock C, Rehli M, Brors B, Schmidl C, Feuerer M, Precursors for Nonlymphoid-Tissue Treg Cells Reside in Secondary Lymphoid Organs and Are Programmed by the Transcription Factor BATF. Immunity. 52, 295–312.e11 (2020). [PubMed: 31924477]

30. Hayatsu N, Miyao T, Tachibana M, Murakami R, Kimura A, Kato T, Kawakami E, Endo TA, Setoguchi R, Watarai H, Nishikawa T, Yasuda T, Yoshida H, Hori S, Analyses of a Mutant Foxp3 Allele Reveal BATF as a Critical Transcription Factor in the Differentiation and Accumulation of Tissue Regulatory T Cells. Immunity. 47, 268–283.e9 (2017). [PubMed: 28778586]

31. Qureshi OS, Zheng Y, Nakamura K, Attridge K, Manzotti C, Schmidt EM, Baker J, Jeffery LE, Kaur S, Briggs Z, Hou TZ, Futter CE, Anderson G, Walker LSK, Sansom DM, Trans-endocytosis of CD80 and CD86: a molecular basis for the cell-extrinsic function of CTLA-4. Science. 332, 600–603 (2011). [PubMed: 21474713]

32. Wing K, Onishi Y, Prieto-Martin P, Yamaguchi T, Miyara M, Fehervari Z, Nomura T, Sakaguchi S, CTLA-4 control over Foxp3+ regulatory T cell function. Science. 322, 271–275 (2008). [PubMed: 18845758]

33. Klocke K, Sakaguchi S, Holmdahl R, Wing K, Induction of autoimmune disease by deletion of CTLA-4 in mice in adulthood. Proc Natl Acad Sci U S A. 113, E2383–2392 (2016). [PubMed: 27071130]
34. Chinen T, Kannan AK, Levine AG, Fan X, Klein U, Zheng Y, Gasteiger G, Feng Y, Fontenot JD, Rudensky AY, An essential role for the IL-2 receptor in Treg cell function. Nat. Immunol. 17, 1322–1333 (2016). [PubMed: 27595233]
35. Fan MY, Low JS, Tanimine N, Finn KK, Priyadharshini B, Germana SK, Kaech SM, Turka LA, Differential Roles of IL-2 Signaling in Developing versus Mature Tregs. Cell Rep. 25, 1204–1213.e4 (2018). [PubMed: 30380412]
36. Toomer KH, Lui JB, Altman NH, Ban Y, Chen X, Malek TR, Essential and non-overlapping IL-2Rα-dependent processes for thymic development and peripheral homeostasis of regulatory T cells. Nat Commun. 10, 1037 (2019). [PubMed: 30833563]
37. Zhou L, Chu C, Teng F, Bessman NJ, Goc J, Santosa EK, Putzel GG, Kabata H, Kelsen JR, Baldassano RN, Shah MA, Sockolow RE, Vivier E, Eberl G, Smith KA, Sonnenberg GF, Innate lymphoid cells support regulatory T cells in the intestine through interleukin-2. Nature. 568, 405–409 (2019). [PubMed: 30944470]
38. Wong HS, Park K, Gola A, Baptista AP, Miller CH, Deep D, Lou M, Boyd LF, Rudensky AY, Savage PA, Altan-Bonnet G, Tsang JS, Germain RN, A local regulatory T cell feedback circuit maintains immune homeostasis by pruning self-activated T cells. Cell, S0092–8674(21)00658–9 (2021).
39. Feng Y, Arvey A, Chinen T, van der Veeken J, Gasteiger G, Rudensky AY, Control of the inheritance of regulatory T cell identity by a cis element in the Foxp3 locus. Cell. 158, 749–763 (2014). [PubMed: 25126783]
40. Li X, Liang Y, LeBlanc M, Benner C, Zheng Y, Function of a Foxp3 cis-element in protecting regulatory T cell identity. Cell. 158, 734–748 (2014). [PubMed: 25126782]
41. Hou J, Schindler U, Henzel WJ, Wong SC, McKnight SL, Identification and purification of human Stat proteins activated in response to interleukin-2. Immunity. 2, 321–329 (1995). [PubMed: 7719937]
42. Jaks V, Barker N, Kasper M, van Es JH, Snippert HJ, Clevers H, Toftgård R, Lgr5 marks cycling, yet long-lived, hair follicle stem cells. Nat Genet. 40, 1291–1299 (2008). [PubMed: 18849992]
43. Strandt H, Pinheiro DF, Kaplan DH, Wirth D, Gratz IK, Hammerl P, Thalhamer J, Stoecklinger A, Neoantigen Expression in Steady-State Langerhans Cells Induces CTL Tolerance. J Immunol. 199, 1626–1634 (2017). [PubMed: 28739880]
44. Harries M, Hardman J, Chaudhry I, Poblet E, Paus R, Profiling the human hair follicle immune system in lichen planopilaris and frontal fibrosing alopecia: can macrophage polarization differentiate these two conditions microscopically? Br J Dermatol. 183, 537–547 (2020). [PubMed: 31883384]
45. Chinen T, Volchkov PY, Chervonsky AV, Rudensky AY, A critical role for regulatory T cell-mediated control of inflammation in the absence of commensal microbiota. J Exp Med. 207, 2323–2330 (2010). [PubMed: 20921284]
46. Scharschmidt TC, Vasquez KS, Pauli ML, Leitner EG, Chu K, Truong H-A, Lowe MM, Sanchez Rodriguez R, Ali N, Laszik ZG, Sonnenburg JL, Millar SE, Rosenblum MD, Commensal Microbes and Hair Follicle Morphogenesis Coordinately Drive Treg Migration into Neonatal Skin. Cell Host Microbe. 21, 467–477.e5 (2017). [PubMed: 28343820]
47. Mobini N, Tam S, Kamino H, Possible role of the bulge region in the pathogenesis of inflammatory scarring alopecia: lichen planopilaris as the prototype. J Cutan Pathol. 32, 675–679 (2005). [PubMed: 16293179]
48. Pozdnyakova O, Mahalingam M, Involvement of the bulge region in primary scarring alopecia. J. Cutan. Pathol. 35, 922–925 (2008). [PubMed: 18537862]
49. Harries MJ, Meyer K, Chaudhry I, E Kloepper J, Poblet E, Griffiths CE, Paus R, Lichen planopilaris is characterized by immune privilege collapse of the hair follicle's epithelial stem cell niche. J. Pathol. 231, 236–247 (2013). [PubMed: 23788005]

50. Ohl L, Mohaupt M, Czeloth N, Hintzen G, Kiafard Z, Zwirner J, Blankenstein T, Henning G, Förster R, CCR7 governs skin dendritic cell migration under inflammatory and steady-state conditions. Immunity. 21, 279–288 (2004). [PubMed: 15308107]
51. Vignali DAA, Collison LW, Workman CJ, How regulatory T cells work. Nat Rev Immunol. 8, 523–532 (2008). [PubMed: 18566595]
52. Collins N, Jiang X, Zaid A, Macleod BL, Li J, Park CO, Haque A, Bedoui S, Heath WR, Mueller SN, Kupper TS, Gebhardt T, Carbone FR, Skin CD4(+) memory T cells exhibit combined cluster-mediated retention and equilibration with the circulation. Nat Commun. 7, 11514 (2016). [PubMed: 27160938]
53. Kobayashi T, Voisin B, Kim DY, Kennedy EA, Jo J-H, Shih H-Y, Truong A, Doebel T, Sakamoto K, Cui C-Y, Schlessinger D, Moro K, Nakae S, Horiuchi K, Zhu J, Leonard WJ, Kong HH, Nagao K, Homeostatic Control of Sebaceous Glands by Innate Lymphoid Cells Regulates Commensal Bacteria Equilibrium. Cell. 176, 982–997.e16 (2019). [PubMed: 30712873]
54. Yang H, Adam RC, Ge Y, Hua ZL, Fuchs E, Epithelial-Mesenchymal Micro-niches Govern Stem Cell Lineage Choices. Cell. 169, 483–496.e13 (2017). [PubMed: 28413068]
55. Schweizer J, Langbein L, Rogers MA, Winter H, Hair follicle-specific keratins and their diseases. Exp Cell Res. 313, 2010–2020 (2007). [PubMed: 17428470]
56. Dikiy S, Li J, Bai L, Jiang M, Janke L, Zong X, Hao X, Hoyos B, Wang Z-M, Xu B, Fan Y, Rudensky AY, Feng Y, A distal Foxp3 enhancer enables interleukin-2 dependent thymic Treg cell lineage commitment for robust immune tolerance. Immunity. 54, 931–946.e11 (2021). [PubMed: 33838102]
57. Nichols LA, Chen Y, Colella TA, Bennet CL, Clausen BE, Engelhard VH, Deletional self-tolerance to a melancyte/melanoma antigen derived from tyrosinase is mediated by a radio-resistant cell in peripheral and mesenteric lymph nodes. J. Immunol. 179, 993–1003 (2007). [PubMed: 17617591]
58. Blattman JN, Grayson JM, Wherry EJ, Kaech SM, Smith KA, Ahmed R, Therapeutic use of IL-2 to enhance antiviral T-cell responses in vivo. Nat Med. 9, 540–547 (2003). [PubMed: 12692546]
59. Petukhova L, Duvic M, Hordinsky M, Norris D, Price V, Shimomura Y, Kim H, Singh P, Lee A, Chen WV, Meyer KC, Paus R, Jahoda CAB, Amos CI, Gregersen PK, Christiano AM, Genome-wide association study in alopecia areata implicates both innate and adaptive immunity. Nature. 466, 113–117 (2010). [PubMed: 20596022]
60. Muñoz-Rojas AR, Mathis D, Tissue regulatory T cells: regulatory chameleons. Nat Rev Immunol. 21, 597–611 (2021). [PubMed: 33772242]
61. Wijeyesinghe S, Beura LK, Pierson MJ, Stolley JM, Adam OA, Ruscher R, Steinert EM, Rosato PC, Vezys V, Masopust D, Expansible residence decentralizes immune homeostasis. Nature. 592, 457–462 (2021). [PubMed: 33731934]
62. Bankhead P, Loughrey MB, Fernández JA, Dombrowski Y, McArt DG, Dunne PD, McQuaid S, Gray RT, Murray LJ, Coleman HG, James JA, Salto-Tellez M, Hamilton PW, QuPath: Open source software for digital pathology image analysis. Sci Rep. 7, 16878 (2017). [PubMed: 29203879]
63. Kovanen PE, Young L, Al-Shami A, Rovella V, Pise-Masison CA, Radonovich MF, Powell J, Fu J, Brady JN, Munson PJ, Leonard WJ, Global analysis of IL-2 target genes: identification of chromosomal clusters of expressed genes. International Immunology. 17, 1009–1021 (2005). [PubMed: 15980098]

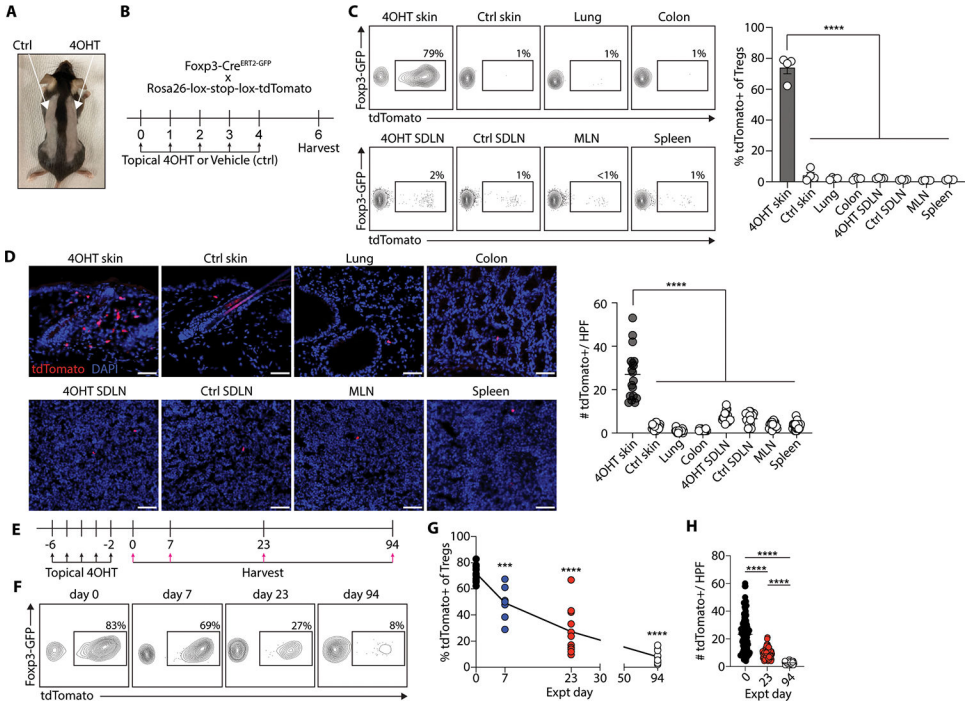

Figure 1. Natural life history of Tregs in skin revealed by localized fate-mapping.

A. Representative photo of a mouse with dorsal back skin shaved in a “mohawk” configuration. **B.** Experimental schematic in which Foxp3^{tdTomato} mice were treated topically for 5 consecutive days with 4OHT on one side of shaved skin or vehicle control (acetone) on the contralateral side, and organs were harvested 2 days after the last treatment. **C.** Representative flow cytometry plots and quantification of % tdTomato+ of Tregs (live CD45+ TCRβ+ CD4+ CD8− Foxp3-GFP+) from the indicated organs following topical 4OHT or vehicle control treatment. SDLN- skin draining lymph node, MLN- mesenteric lymph node. **D**. Representative medium-power images of tissue sections from the indicated organs following the treatment regimen outlined in (**B**) (bar = 50 μm); quantification of # tdTomato+ cells per high powered field (HFP). **E**. Experimental schematic which Foxp3^{tdTomato} mice were treated topically for 5 consecutive days with 4OHT on shaved skin and skin was harvested at the indicated time points. **F, G**. Representative flow cytometry plots (**F**) and quantification (**G**) of % tdTomato+ of skin Tregs at the indicated time points. Statistics were calculated as a comparison to the day 0 timepoint. **H**. Quantification of # tdTomato+ cells per high powered field (HFP) in skin sections from the indicated time points. Data in **C** and **D** are representative of two independent experiments with similar results. Data in **F**, **G**, and **H** are pooled from two independent experiments. Results are shown as individual data points and mean +/− s.e.m (**C**) or individual data points and mean (**D, G, H**). Statistics are calculated by one-way ANOVA with Tukey’s test for multiple comparisons. ***$p < 0.001$, ****$p < 0.0001$.

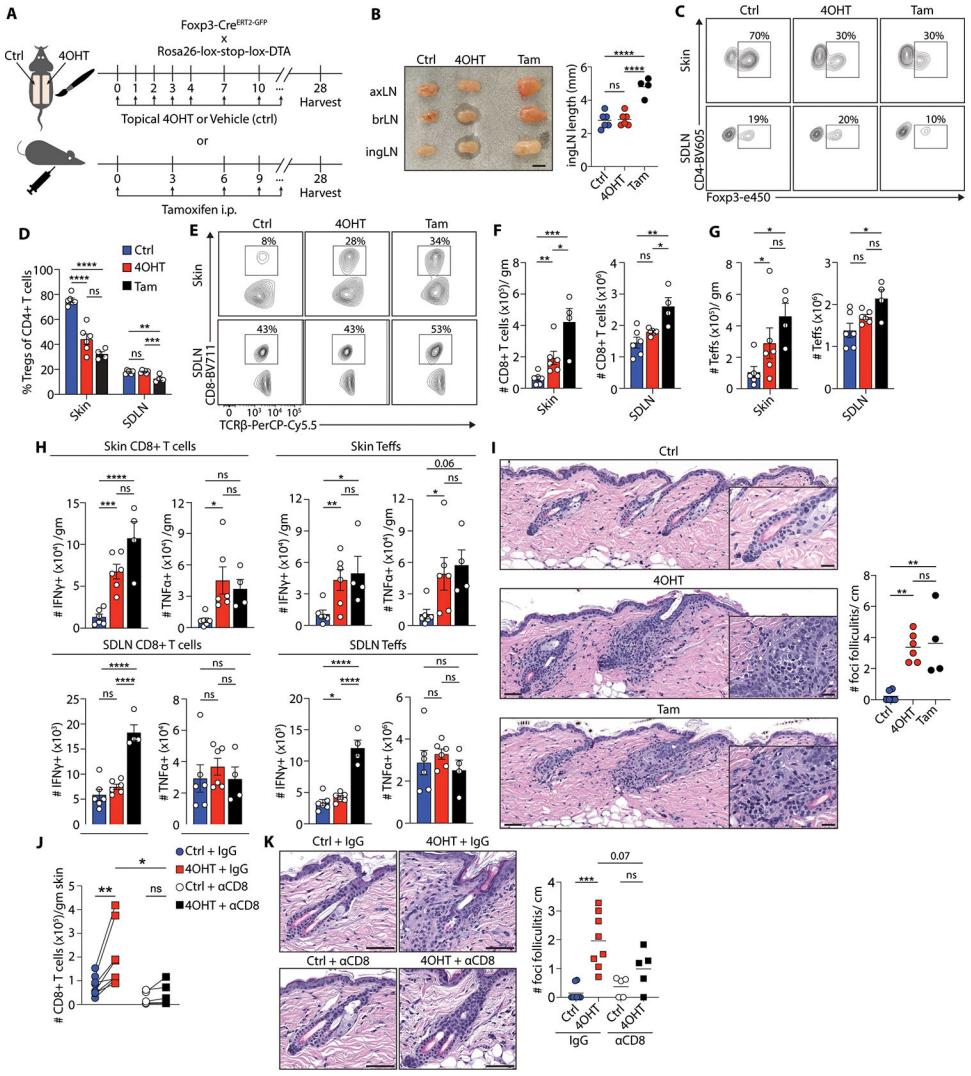

Figure 2. Skin regulatory T cells suppress hair follicle-associated inflammation.

A. Experimental schematic in which Foxp3^{iDTA} mice were treated for 5 consecutive days with 4OHT on one side of shaved back skin and vehicle control (acetone) on the contralateral side and every three days thereafter for 4 weeks. A separate group of Foxp3^{iDTA} mice were treated with intraperitoneal injection of Tamoxifen every three days for 4 weeks. Skin and skin draining lymph nodes (SDLN) were harvested at 4 weeks. **B**. Representative photo of SDLN (axLN: axillary, brLN: brachial, ingLN: inguinal) from Foxp3^{iDTA} mice that underwent the indicated treatments; bar= 2 mm (left). Quantification of ingLN length measurements (right). **C, D**. Representative flow cytometry plots and quantification of % Tregs. **E, F**. Representative flow cytometry plots and quantification of # CD8+ T cells. **G**. Quantification of # Teffs (CD4+ Foxp3−). **H**. Quantification of pro-inflammatory cytokine production by CD8+ T cells and Teffs in skin and SDLN of Foxp3^{iDTA} mice (interferon-γ: IFNγ, tumor necrosis factor-α: TNFα). **I**. Representative photomicrographs of dorsal back skin histology sections of Foxp3^{iDTA} mice that underwent the indicated treatment (bar= 50 μm); inset: higher magnification of hair follicle (bar= 20 μm), and quantification of # foci of hair follicle-associated inflammation (folliculitis). **J**.

Quantification of # CD8+ T cells in skin. Mice underwent the topical treatment regimen as depicted in (**A**) and were concurrently treated with intraperitoneal injections of control IgG or anti-CD8 depleting antibody every 5 days. **K**. Representative photomicrographs of histology during the indicated treatment conditions (bar = 50 μm), and quantification of # folliculitis foci in skin under the indicated treatment conditions. Data in **B-K** are representative of two independent experiments with similar results. Results are shown as individual data points and mean (**B, I, K**), individual data points and mean +/− s.e.m (**D, F, G, H**), or paired data points (**J**). Statistics are calculated by one-way ANOVA with Tukey's test for multiple comparisons (**B, D, F, and H (Tam comparison), and I**), two-way ANOVA (**J and K: 4OHT vs. 4OHT comparison**), and paired two-tailed Student's *t*-test (**B, D, F-H, K (ctrl vs. 4OHT comparison)**). *$p < 0.05$, **$p < 0.01$, ***$p < 0.001$, ****$p < 0.0001$, ns = not significant.

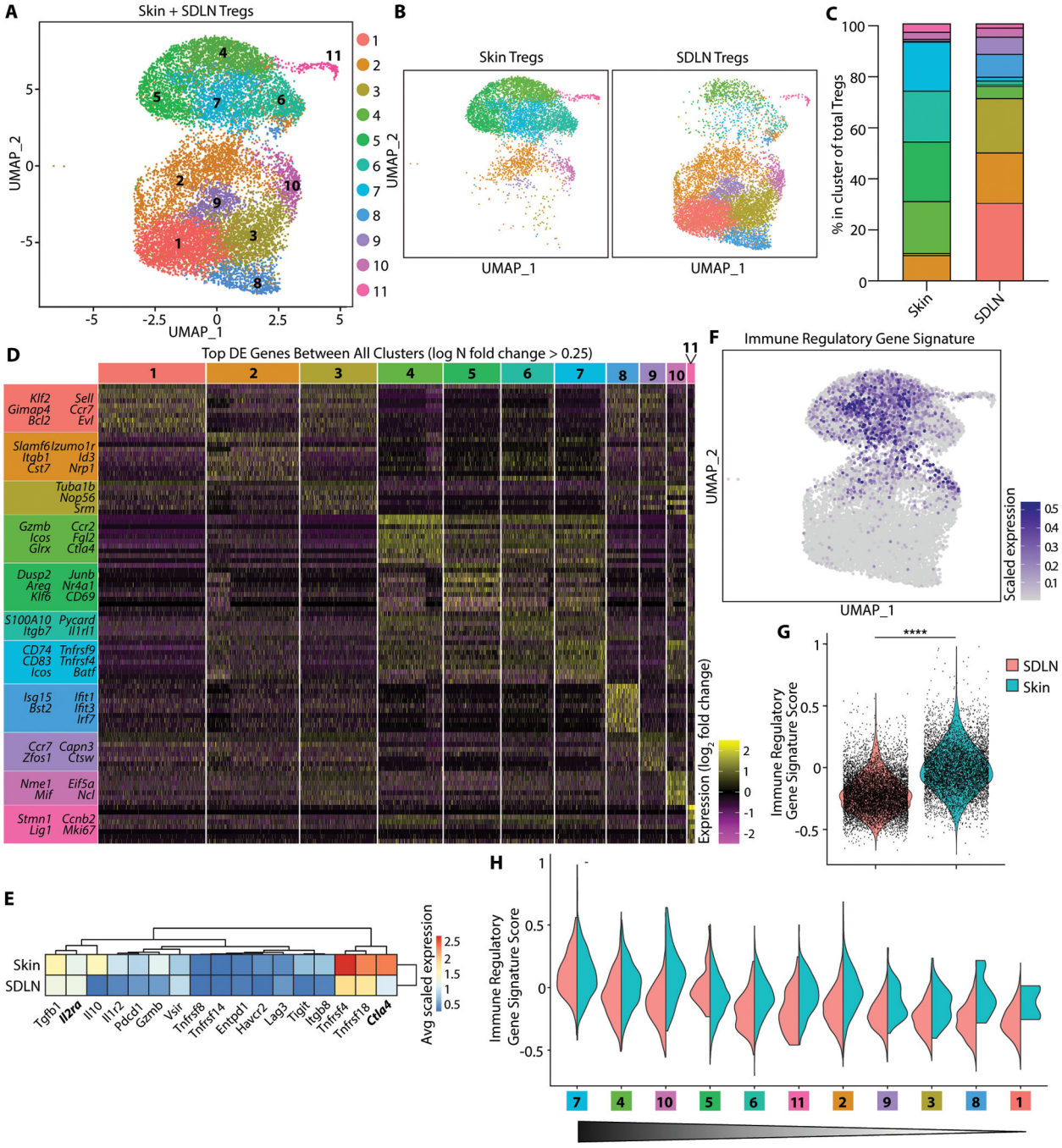

Figure 3. Skin Tregs exhibit a heightened immunoregulatory gene signature.

(**A to F and H**) scRNAseq of sort-purified T_{regs} (gating: live $CD45^+$ $TCR\beta^+$ $CD4^+$ $CD8^-$ GFP^+ cells) from dorsal back skin and SDLNs of adult Foxp3-$Cre^{ERT2\text{-}GFP}$ mice. (**A and B**) Unsupervised clustering of combined (A) and separate skin and SDLN T_{reg} scRNAseq data (**B**). (**C**) Graphical summary of the frequency of T_{regs} in each cluster according to tissue. (**D**) Heatmap displaying the top 10 differentially expressed (DE) genes for each cluster when comparing clusters 1 to 11 (ranked by fold change). (**E**) Heatmap of select genes involved in immune tolerance/immunoregulation. (**F**) Feature plot displaying the immune regulatory

gene signature in combined skin and SDLN scRNAseq data. (**G**) Violin plot of the immune regulatory gene signature split by tissue. (**H**) Violin plots of the immune regulatory gene signature in each individual cluster split by tissue type. Horizontal triangle in grayscale denotes decreasing expression score moving left to right. Data are representative of one experiment (**A to H**). Statistics were calculated by unpaired Wilcoxon rank sum test of SDLN T_{regs} pooled from two mice and skin T_{regs} pooled from four mice (G). ****$P <$ 0.0001.

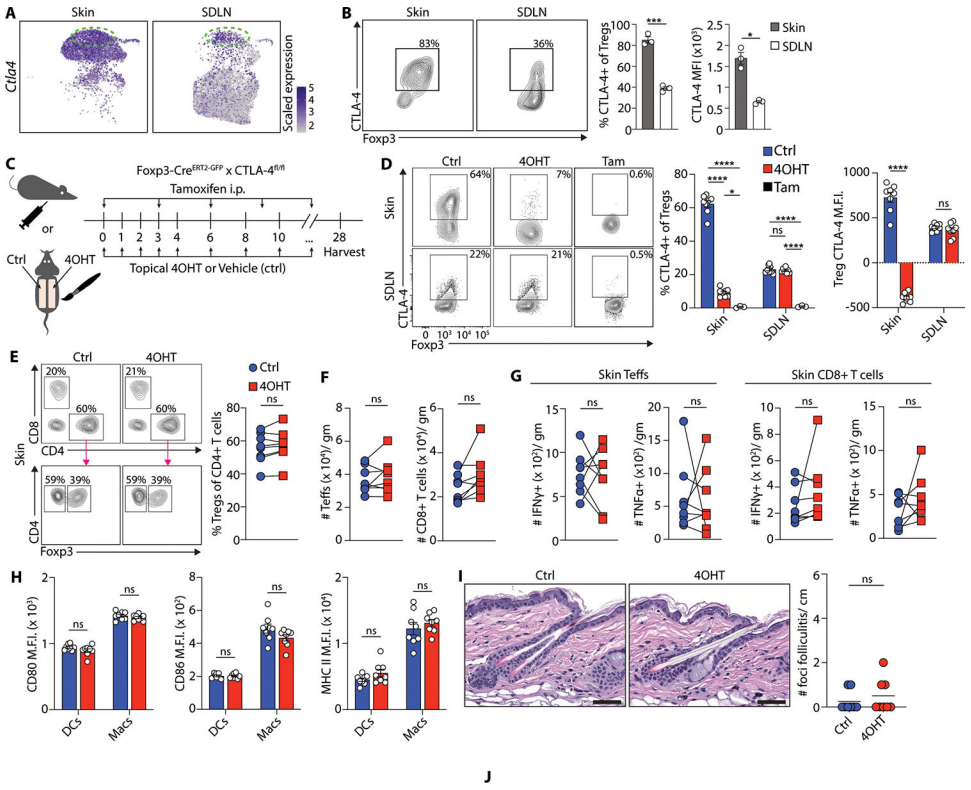

Figure 4. CTLA-4 expression on skin Tregs is dispensable for immune homeostasis.

(**A**) Feature plots of *Ctla4* gene expression in skin and SDLN T_{regs}. Dashed oval indicates relative location of cluster 4 (Fig. 3A). (**B**) Representative flow cytometry plots and quantification of the frequency and expression level of CTLA-4 on skin and SDLN T_{regs}.(**C**) Experimental schematic in which Foxp3$^{\Delta CTLA-4}$ mice were treated for five consecutive days with 4OHT on one side of shaved back skin and vehicle control (acetone) on the contralateral side and every 2 days thereafter for 4 weeks. A separate group of Foxp3$^{\Delta CTLA-4}$ mice was treated with intraperitoneal injection of tamoxifen every 3 days for 4 weeks. Skin and SDLNs were harvested at 4 weeks. (**D**) Representative flow cytometry plots and quantification of % CTLA-4$^+$ T_{regs} and mean fluorescence intensity (MFI) of CTLA-4 expression on T_{regs}. (**E**) Representative flow cytometry plots and gating of CD8$^+$ T cells, T_{effs}, and T_{regs} and quantification of the frequency of T_{regs}. (**F**) Quantification of number of T_{effs} and CD8$^+$ T cells. (**G**) Quantification of proinflammatory cytokine production by CD8$^+$ T cells and T_{effs} in skin. (**H**) Quantification of MFI of CD80, CD86, and MHCII expression on DCs (live CD45$^+$ TCRβ$^-$ CD3ε$^-$ MHCII$^+$ CD64$^-$ CD11c$^+$) or macrophages (Macs; live CD45$^+$ TCRβ$^-$ CD3ε$^-$ MHCII$^+$ CD64$^+$ CD11c$^-$). (**I**) Representative photomicrographs of dorsal back skin histology sections of Foxp3$^{\Delta CTLA-4}$ mice that underwent the indicated topical treatment (scale bar, 50 μm) and quantification of the number of foci of HF-associated inflammation (folliculitis). Data in (A) to (I) are representative of two independent experiments with similar results. Results are shown as individual data points and mean ± SEM (B, D, and H), paired data points (E to G), or individual data points and mean (I). Statistics were calculated by unpaired two-tailed Student's t test (B and I), paired two-tailed Student's *t* test (D to H; ctrl versus 4OHT

comparison), or one-way ANOVA with Tukey's test for multiple comparisons (D; Tam comparison). *$P < 0.05$, ***$P < 0.001$, and ****$P < 0.0001$. ns, not significant.

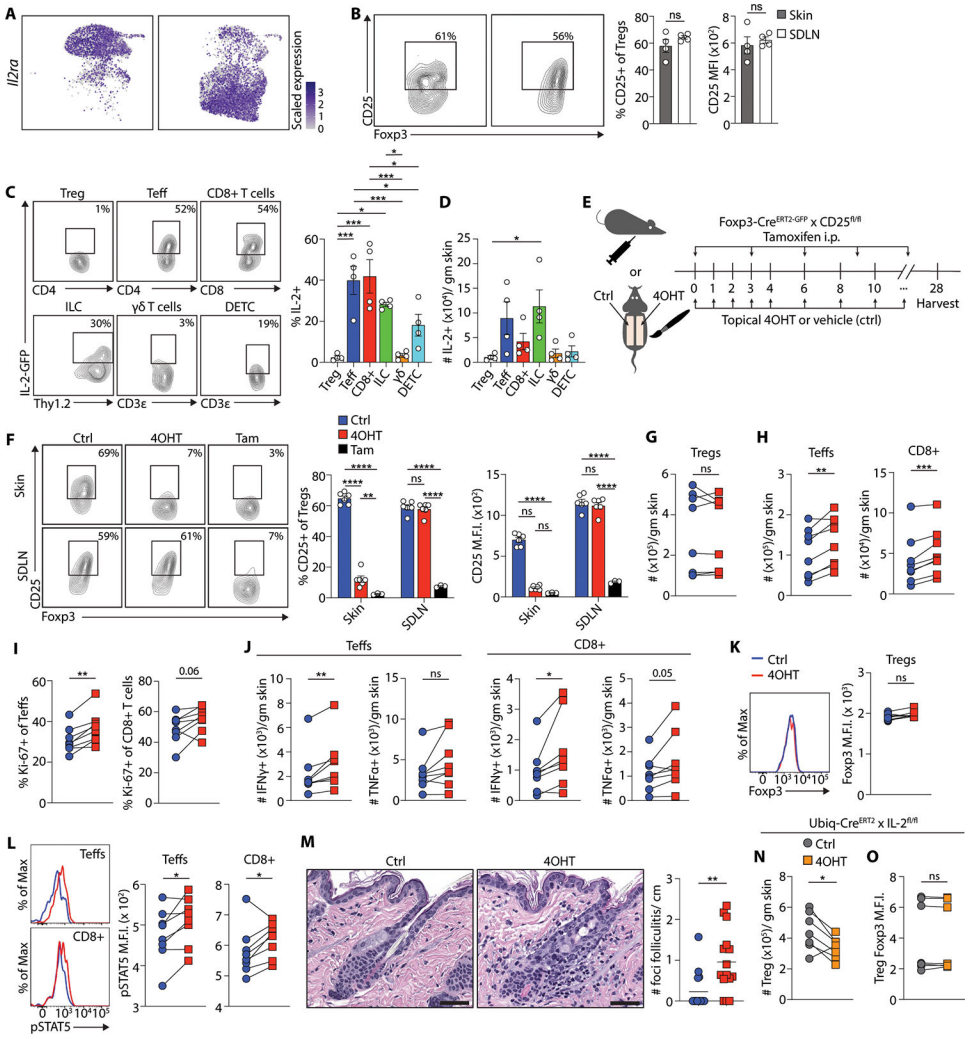

Figure 5. CD25 expression on skin Tregs restrains hair follicle-associated inflammation.

(**A**) Feature plots of *Il2ra* gene expression in skin and SDLN T_{regs}. (**B**) Representative flow cytometry plots and quantification of the frequency and expression level of CD25 on skin and SDLN T_{regs}. (**C** and **D**) Representative flow cytometry plots and quantification of % and number of IL-2 expression in lymphocyte subsets from skin of IL-2–GFP reporter mice. IL-2–GFP^+ gates were set according to wild-type C57Bl/6 controls. (**E**) Experimental schematic in which $Foxp3^{\Delta CD25}$ mice were treated for five consecutive days with 4OHT on one side of shaved back skin and vehicle control (acetone) on the contralateral side and every 2 days thereafter for 4 weeks. A separate group of mice was treated with intraperitoneal injection of tamoxifen every 3 days for 4 weeks. Skin and SDLNs were harvested at 4 weeks. (**F**) Representative flow cytometry plots and quantification of % $CD25^+$ T_{regs} and mean fluorescence intensity (MFI) of CD25 expression on T_{regs}. (**G** and **H**) Quantification of # T_{regs}, T_{effs}, and $CD8^+$ T cells. (**I**) Quantification of the proliferation index (% Ki-67^+) of T_{effs} and $CD8^+$ T cells. (**J**) Quantification of proinflammatory cytokine production by T_{effs} and $CD8^+$ T cells. (**K**) Representative flow cytometry histogram plot and quantification of Foxp3 MFI in skin T_{regs}. (**L**) Representative flow cytometry histogram plots and quantification of pSTAT5 MFI in skin T_{effs} and $CD8^+$ T cells. (**M**)

Representative photomicrographs of dorsal back skin histology sections of $Foxp3^{\Delta CD25}$ mice that underwent the indicated topical treatment (scale bar, 50 μm) and quantification of number of foci of hair follicle–associated inflammation (folliculitis). (N and O) Ubiq-Cre^{ERT2} × IL-$2^{fl/fl}$ mice were shaved in a mohawk configuration and treated with topical 4OHT or vehicle control for 4 weeks as in (C). (**N**) Quantification of # T_{regs} in skin. (**O**) Quantification of Foxp3 MFI in skin T_{regs}. Data in (A) to (L) are representative of two independent experiments with similar results. Data in (M) to (O) show pooled data from two independent experiments. Results are shown as individual data points and mean ± SEM (B, C, D, and F), paired data points (G to L, N, and O), or individual data points and mean (M). Statistics were calculated by unpaired two-tailed Student's *t* test (B and M), paired two-tailed Student's *t* test (F to L, N, and O; ctrl versus 4OHT comparison), or one-way ANOVA with Tukey's test for multiple comparisons [C, D, and E; Tam comparison (F)]. $*P < 0.05$, $**P < 0.01$, $***P < 0.001$, and $****P < 0.0001$. ns, not significant.

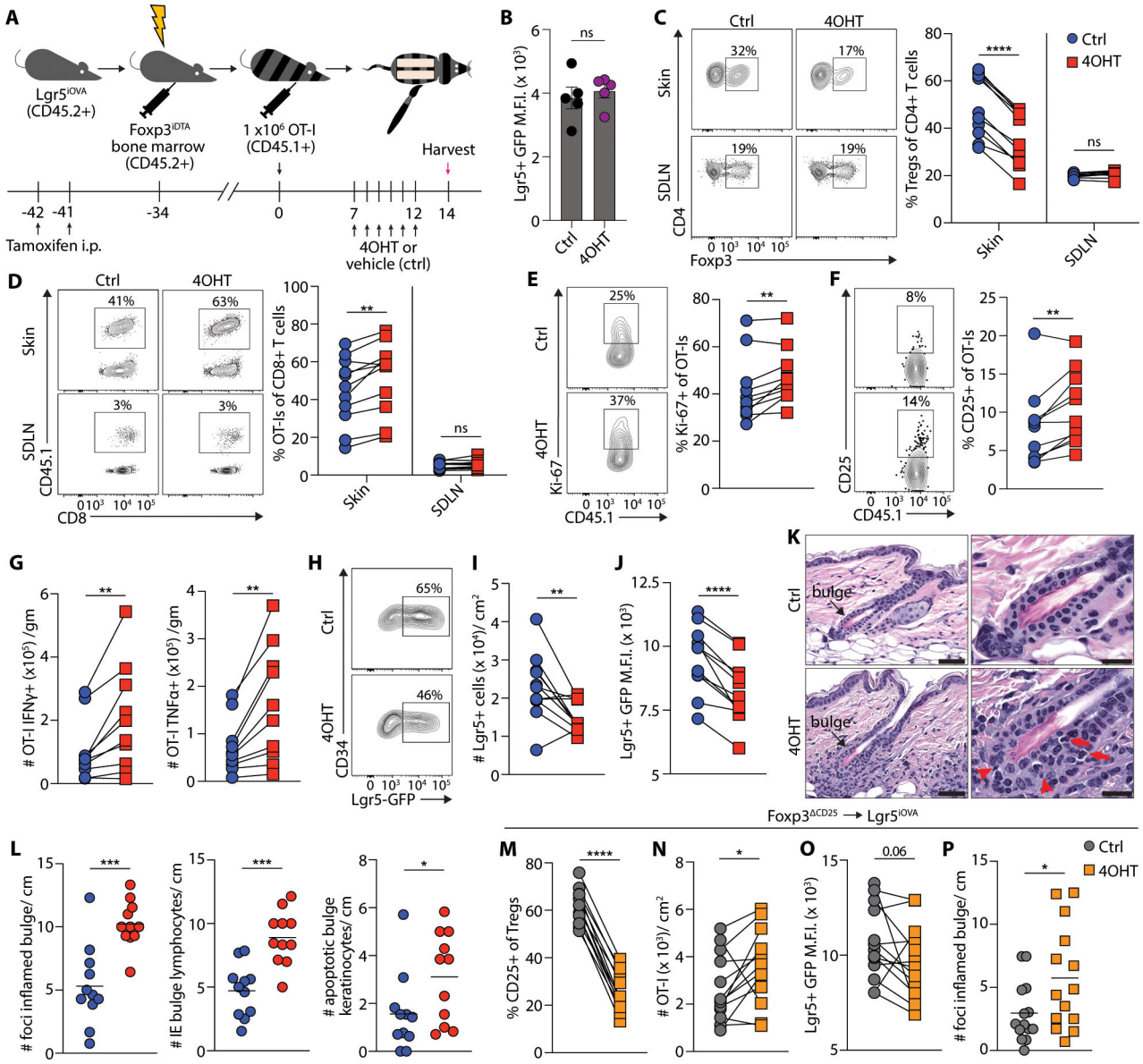

Figure 6. Skin Tregs restrain autoimmune attack of hair follicle stem cells.

A. Schematic and model of experimental timeline in which bone marrow from Foxp3^{iDTA} donor mice was transferred to irradiated OVA-expressing Lgr5^{iOVA} recipients. Lgr5^{iOVA} mice were treated with Tamoxifen intraperitoneally (i.p.) for two consecutive days to induce OVA in bulge hair follicle stem cells (HFSCs), followed by irradiation and transfer of 1 × 10^7 Foxp3^{iDTA} bone marrow cells. Following bone marrow reconstitution, chimeric mice underwent adoptive transfer of 1 × 10^6 OT-I T cells (CD45.1+). One week after OT-I T cell transfer, mice were shaved in a mohawk configuration and topical 4OHT or vehicle was applied for 5 consecutive days. Skin and skin draining lymph nodes (SDLN) were harvested 2 days thereafter. **B**. Quantification of the mean fluorescence intensity (M.F.I.) of GFP expression in Lgr5+ cells (gated on live, CD45−, Sca-1- EpCAM^{int} CD34+) from Lgr5^{iOVA} mice that were treated with the Tamoxifen and 4OHT regimen and harvested on day 14 as described in (**A**). **C**. Representative flow cytometry plots and quantification of

% skin Tregs. **D**. Representative flow cytometry plots and quantification of % skin OT-I T cells. **E, F**. Representative flow cytometry plots and quantification of % Ki-67 and CD25 of OT-I T cells. **G**. Quantification of interferon-γ (IFNγ) and tumor necrosis factor-α (TNFα) producing skin OT-I T cells. **H, I**. Representative flow cytometry plots and quantification of % and # of Lgr5-GFP+ HFSCs. **J**. Quantification of M.F.I. of GFP in Lgr5+ cells. **K**. Representative medium- and high-powered views from photomicrographs of dorsal back skin histology sections of chimeric mice; bar= 50 μm (left panels) and 20 μm (right panels). Arrowheads indicate apoptotic bulge keratinocytes and arrows indicate intraepithelial bulge lymphocytes. **L**. Quantification of # foci of bulge-associated inflammation, intraepithelial (IE) bulge lymphocytes, and apoptotic bulge keratinocytes. **M-P**. Experimental results utilizing $Foxp3^{\Delta CD25} \rightarrow Lgr5^{iOVA}$ chimeric mice with quantification of % CD25 on skin Tregs (**M**), # skin epithelial OT-I T cells (**N**), GFP M.F.I. in Lgr5-GFP+ cells (**O**), and foci of bulge-associated inflammation (**P**). Data in **A-L** are representative of two independent experiments with similar results. Data in **M-P** shows pooled data from two independent experiments. Results are shown as individual data points and mean +/− s.e.m (**B**), paired data points (**C-G, I-J, and M-O**) or individual data points and mean (**L, P**). Statistics are calculated by paired two-tailed Student's *t*test (**C-G, I-J, and M-O**), or unpaired two-tailed Student's *t*-test (**L, P**). $^{**}p < 0.01$, $^{***}p < 0.001$, $^{****}p < 0.0001$, ns = not significant.

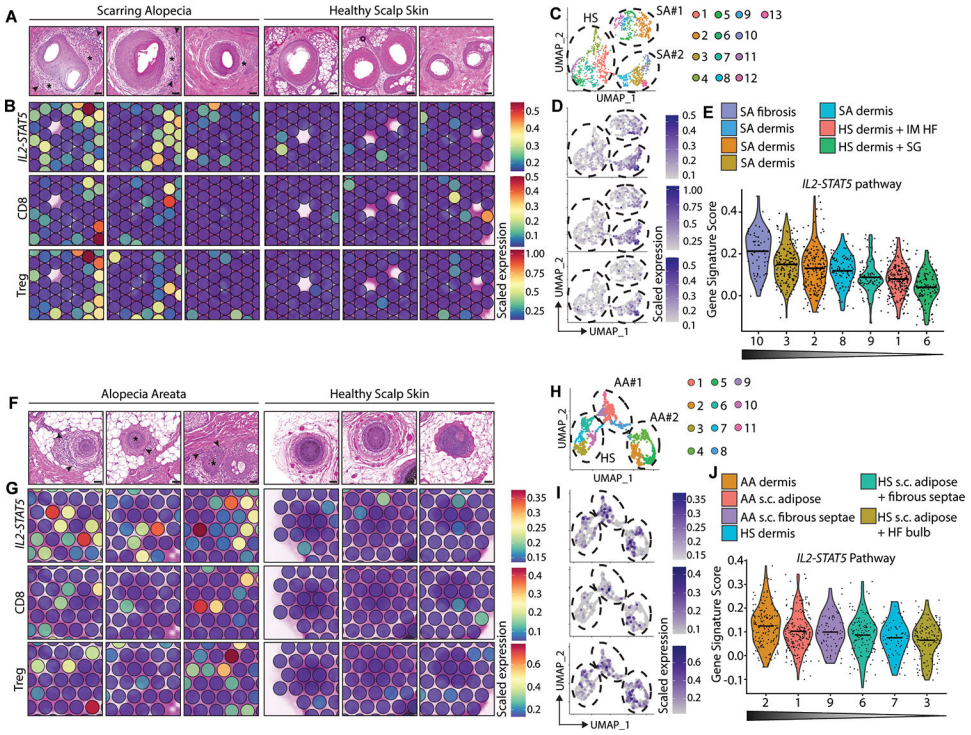

Figure 7. Human autoimmune alopecia demonstrates a heightened IL-2 signaling gene signature around hair follicles.

A, E. Medium-power photomicrographs of hematoxylin and eosin (H&E) stained tissue sections representative of regions of pathology in human scarring alopecia (SA), alopecia areata (AA) and corresponding regions in healthy scalp skin (HS) as denoted by the dashed boxes in Figure S9B and S10A. In (**A**), arrowheads indicate lymphocytic inflammation around hair follicles, and asterisks indicate perifollicular fibrosis. In (**E**), arrowheads indicate lymphocytic inflammation around hair follicles, and asterisks indicate involutional hair follicles. Bar = 50 μm. **B, F**. Medium-power images of spatial transcriptomic (ST) feature plots of the *IL2-STAT5* pathway, and CD8 and Treg gene signatures superimposed on the corresponding H&E images in (**A**) and (**E**). **C, H**. Unsupervised clustering of ST data from two samples of SA and two samples of HS, and two samples of AA and two samples of HS as demonstrated in Figure S9C and S10B. **D, I**. Feature plots of SA, AA, and HS spatial transcriptomic data displaying the *IL2-STAT5* pathway, and CD8 T cell and Treg gene signatures. **E, J**. Violin plots of the *IL2-STAT5* pathway in ST clusters representative of microanatomic stromal niches in diseased and healthy skin. Bar represents mean. Horizontal triangle in greyscale denotes decreasing expression score moving left to right. Data are representative of one independent 10X Visium capture area each for the scarring alopecia TMA sample and the alopecia areata TMA sample.